The duration and magnitude of Cretaceous cool events

Evidence from the northern high latitudes

Vickers, Madeleine; Price, Gregory; Jerrett, Rhodri; Sutton, Paul; Watkinson, Matthew; FitzPatrick, Meriel

Published in:
Geological Society of America Bulletin

DOI:
10.1130/B35074.1

Publication date:
2019

Document version
Version created as part of publication process; publisher's layout; not normally made publicly available

The duration and magnitude of Cretaceous cool events: Evidence from the northern high latitudes

Madeleine L. Vickers[1,†], Gregory D. Price[2,†], Rhodri M. Jerrett[3], Paul Sutton[2], Matthew P. Watkinson[2], and Meriel FitzPatrick[2]

[1]*Department of Geosciences and Natural Resource Management, Københavns Universitet, Øster Voldgade 10, 1350 Copenhagen, Denmark*

[2]*Centre for Research in Earth Sciences, School of Geography, Earth and Environmental Sciences, Plymouth University, Drake Circus, Plymouth PL4 8AA, UK*

[3]*School of Earth and Environmental Sciences, University of Manchester, Oxford Road, Manchester M13 9PL, UK*

ABSTRACT

The Early Cretaceous (145–100 Ma) was characterized by long-term greenhouse climates, with a reduced equatorial to polar temperature gradient, although an increasingly large body of evidence suggests that this period was punctuated by episodic global "cold snaps." Understanding climate dynamics during this high-atmospheric CO2 period of Earth's history may have significant impact on how we understand climatic feedbacks and predict future global climate changes under an anthropogenically-driven high-pCO2 atmosphere. This study utilizes facies analysis to constrain the paleobathymetry of Lower Cretaceous glendonites—a pseudomorph after ikaite, a mineral that forms naturally at 7 °C or lower—from two paleo-high-latitude (60–70°N) sites in Svalbard, Arctic Norway, to infer global climatic changes during the Early Cretaceous. The original ikaite formed in the offshore transition zone of a shallow marine shelf at water depths of <100 m, suggesting mean annual water temperatures of ≤7 °C at these depths at 60–70°N. We correlate glendonite-bearing horizons from Lower Cretaceous successions around the globe using carbon isotope stratigraphy, in conjunction with the pre-existing biostratigraphic framework, in order to infer northern hemispheric to global climatic cooling. A distinct interval of glendonites in the Northern Hemisphere, from sites >60°N, spans the late Berriasian to earliest Barremian (at least 8.6 m.y.), significantly prolonging the duration of the previously hypothesized Valanginian cold snap (associated with the "Weissert Event"). Widespread glendonites occur again in late Aptian and extend to the early Albian, in both hemispheres, corroborating other proxy evidence for late Aptian cooling. The glendonites from Svalbard suggest that Cretaceous cold episodes were characterized with high latitude (>60°N) shallow water temperatures that are consistent with the existence of a small northern polar ice cap at this time.

INTRODUCTION

The Early Cretaceous was characterized by high atmospheric CO_2 levels, and a long-term greenhouse climate (e.g., Wang et al., 2014 and references therein). Significantly lower than modern pole-to-equator temperature gradients are suggested by various paleothermometers (e.g., Littler et al., 2011; Price and Passey, 2013), but these are not always reproduced in climate models (e.g., Fluteau et al., 2007; Hunter et al., 2013). However, many studies suggest that short episodes of cooling punctuated this greenhouse trend (e.g., by marked changes in floral and faunal assemblages; changes in stable oxygen record of marine calcifiers; sharp falls in sea level, Pucéat et al., 2003; Erba and Tremolada, 2004; Harland et al., 2007; McArthur et al., 2007; Mutterlose et al., 2009; Maurer et al., 2013; McAnena et al., 2013; Price and Passey, 2013; Bodin et al., 2015), often reflected in perturbations in the stable carbon isotopic record (e.g., Menegatti et al., 1998; Weissert and Erba, 2004; McArthur et al., 2007; Bodin et al., 2015; Price et al., 2016). Cretaceous positive carbon-isotope excursions have been linked directly with episodes of increased organic carbon burial whereby the leaching of nutrients on coastal lowlands during a rise in sea-level, possibly triggered by globally warmer temperatures, resulted in increased ocean fertilization and productivity (e.g., Erba et al., 2004; Weissert and Erba, 2004). A consequence of increased organic carbon burial is removal of CO_2 from the atmosphere and the onset of cooling, typically coinciding with peak $\delta^{13}C$ values, and followed by an interval waning of $\delta^{13}C$ values (e.g., Lini et al., 1992). The magnitude of warming and cooling is still debated, as the various climate proxies do not necessarily agree with model predictions, or each other, particularly with respect to polar climates (Bice et al., 2003; Jenkyns et al., 2004; Littler et al., 2011; Price and Passey, 2013). Furthermore, there is ongoing debate as to whether temperatures were ever low enough for small polar ice-caps to develop, with possible glacial or ice-rafted sediments being reported from the high, and even mid latitudes (e.g., Frakes et al., 1995; Rodríguez-López et al., 2016). Understanding the climate dynamics of this high-pCO_2 Earth, and getting agreement between proxy evidence and general circulation model (GCM) simulations, is important for predicting future climate change using GCM simulations.

Additional evidence for cooling includes widespread glendonite (pseudomorphs after marine sedimentary ikaite) occurrence in paleo-high latitude sediments (Fig. 1; Nagy, 1970; Kemper, 1987; De Lurio and Frakes, 1999; Maher et al., 2004; Price and Nunn, 2010; Herrle et al., 2015; Vickers et al., 2016; Grasby et al., 2017; Rogov et al., 2017). Glendonites are regarded as cold-water indicators as their precursor mineral, ikaite, generally requires temperatures below 7 °C to grow in natural, marine sedimentary settings (e.g., Suess et al., 1982; Bischoff et al., 1993; Buchardt et al., 2001; Swainson and Hammond, 2001; Greinert and Derkachev, 2004; Zhou et al., 2015). While laboratory experiments have produced ikaite at higher temperatures (e.g., Purgstaller et al., 2017; Stockmann et al., 2018), these experiments do not represent the chemical

†*mlv@ign.ku.dk, g.price@plymouth.ac.uk.*

https://doi.org/10.1130/B35074.1; 7 figures; 2 tables; Data Repository item 2019166.

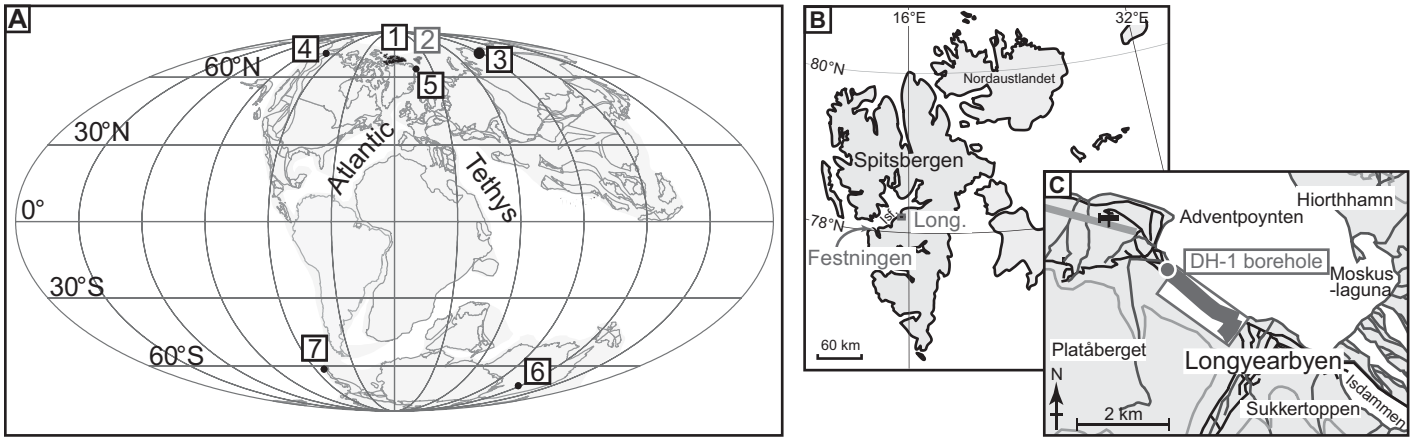

Figure 1. (A) Early Cretaceous paleogeography for the Northern Hemisphere, reproduced from Boucot et al. (2013). Locations of Lower Cretaceous glendonite-bearing sites marked: (1) Queen Elizabeth Islands (Kemper and Schmitz, 1975; Kemper and Schmitz, 1981; Kemper, 1987; Lippert, 2004; Herrle et al., 2015; Grasby et al., 2017); (2) Svalbard archipelago, Norway (this study); (3) Northern Russia (Rogov et al., 2017); (4) Canning River, Alaska, USA (van der Kolk et al., 2011); (5) Kilen, North Greenland (Hovikoski et al., 2018); (6) Eromanga Basin, Australia (Frakes et al., 1995; De Lurio and Frakes, 1999); (7) South Shetland Islands (Rogov et al., 2017). (B) Map of Svalbard, from Vickers et al. (2018). (C) Map of area around Longyearbyen, reproduced from toposvalbard.npolar.no. Airport Road section indicated as red line. Long.—Longyearbyen; Isf.—Isfjorden.

conditions found in natural sedimentary marine ikaite-bearing settings (e.g., fig. 8, p. 140 of Purgstaller et al., 2017). A traditionally poor estimation of the paleobathymetries at which documented glendonites formed, and a lack of high-resolution age constraints for glendonite-bearing horizons which inhibits their supra-regional correlation, diminish the paleoclimatic significance of these cold-water proxies. Therefore, this study sets out to constrain the paleobathymetry and relative age of Lower Cretaceous "cold water" glendonites from two paleo-high-latitude (~60–70°N) sites in Svalbard, Arctic Norway. The former is achieved using conventional facies analysis, and the latter via high-resolution carbon isotope stratigraphy underpinned by biomarker and palynofacies analysis. This provides the opportunity to better assess the paleoclimatic significance of glendonites, by correlating their occurrences with other glendonite horizons across the globe, and with hypothesized global climatic cooling events throughout the Early Cretaceous.

Geological Setting

The Svalbard archipelago of Norway is part of the greater Barents Sea region, located between 74°N and 81°N on the northwestern corner of the Barents Shelf, and the principal island is Spitsbergen. During the Early Cretaceous, the Barents Sea was part of the larger Boreal Sea (which included the Canadian Queen Elizabeth Islands, northern Alaska, USA, and NE Greenland), prior to the opening of the Atlantic in the Cenozoic (Harland et al., 1984). Thus, Svalbard, along with the Canadian Arctic and parts of Russia, were among the highest northerly landmasses (Fig. 1). From the Berriasian to Hauterivian, sedimentation on Svalbard was characterized by deposition of mud and subordinate sand in an offshore marine shelf setting (Rurikfjellet Formation; Harland and Kelly, 1997; Johnsen et al., 2001; Dypvik et al., 2002; Polteau et al., 2016), with an emergent land mass some 300 km to the south-west (Harland and Kelly, 1997; Johnsen et al., 2001; Dypvik et al., 2002). Regional uplift and doming, associated with emplacement of the High Arctic Large Igneous Province (HALIP; Maher, 2001; Nejbert et al., 2011; Senger et al., 2014) began in the northwest during the latest Hauterivian–earliest Barremian, and progressed south-eastward through Svalbard through the middle Barremian, resulting in an episode of hiatus and erosion (e.g., Gjelberg and Steel, 1995). Renewed subsidence from the late Barremian onwards resulted in the deposition of fluvio-deltaic sandstones, subordinate conglomerate, mudstone, and coal of the Helvetiafjellet Formation, which lies unconformably over the Rurikfjellet Formation (Gjelberg and Steel, 1995; Harland and Kelly, 1997; Worsley, 2008; Midtkandal et al., 2008). This subaerial unconformity is most clearly developed in north-westerly locations on Spitsbergen (Fig. 2; Gjelberg and Steel, 1995; Midtkandal et al., 2008), but whether the uplift and erosion was sufficient to generate significant disconformity between the marine and deltaic sediments across the whole of Svalbard is debated (e.g., Grøsfjeld, 1992). During the late Barremian to early Aptian, these delta plain environments dominated sedimentation on Spitsbergen, which supported vegetated swamps and ornithopod dinosaurs (Lapparent, 1962; Hurum et al., 2006; Hurum et al., 2016). Regional relative sea-level rise in the Aptian to Albian resulted in transgression of the delta plain, and re-establishment of marine conditions with deposition of shelf mudstones and sandstones of the Carolinefjellet Formation (Nagy, 1970; Gjelberg and Steel, 1995; Dypvik et al., 2002; Midtkandal and Nystuen, 2009). The succession was intruded by a suite of doleritic sills and dykes during deposition, also associated with HALIP magmatism (the Diabasodden Suite; Nejbert et al., 2011). Crustal shortening between Greenland and Svalbard from the Late Cretaceous onward resulted in complete subaerial exposure, and deformation of the Early Cretaceous and older strata into a major S-plunging eastwardly vergent inclined syncline (the Central Basin syncline). Upper Cretaceous strata are wholly absent in Svalbard, and Cenozoic sediments rest unconformably over the Mesozoic succession (Harland and Kelly, 1997).

METHODS

Two localities on the island of Spitsbergen preserving Lower Cretaceous sediments were chosen for this study (Fig. 1). The first is

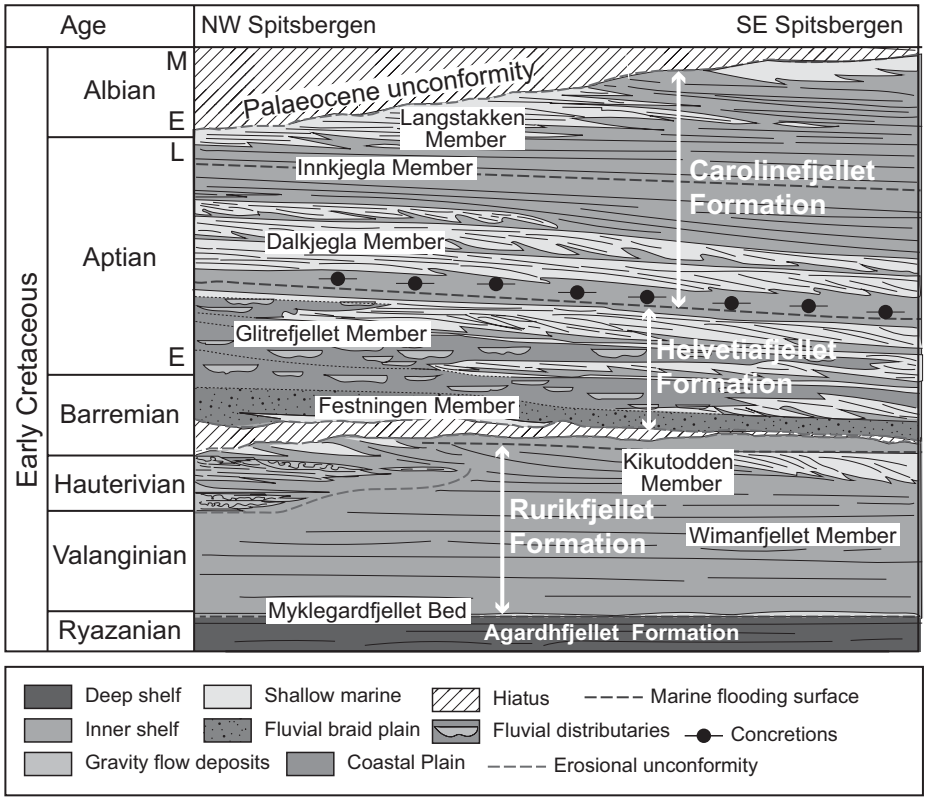

Figure 2. Stratigraphic cross-section and the regional development of the Lower Cretaceous part of the Adventdalen Group across Spitsbergen, Norway after Grundvåg et al. (2017). E—early; M—middle; L—late.

located along the foreshore at Festningen, on the southwestern side of Isfjorden (78°09.98′N, 13°94.32′E), on the vertical western limb of the Central Basin syncline (hereafter referred to as the Festningen section). The Festningen section has been studied extensively by geologists since the early 1900s (early work was summarized by Hoel and Ørvin, 1937), and it is a standard reference for Svalbard's geology (e.g., Mørk and Worsley, 2006). The site is also the stratotype for the distinctive fluvio-deltaic sandstones of the Festningen Member (Mørk et al., 1999). The Festningen section is particularly useful for this study as the entire Lower Cretaceous succession outcrops here; subvertically bedded along 5–10 m high cliffs, with exposure close to 100% (Fig. 1). All formal lithostratigraphic units of the Lower Cretaceous of Spitsbergen occur here (Hoel and Ørvin, 1937; Steel et al., 1978; Mørk et al., 1999; Hurum et al., 2006; Midtkandal et al., 2016), so it is therefore also important for the purposes of comparing to previous studies. The second is a series of road- and stream-cut exposures of the Carolinefjellet Formation along the road between the town of Longyearbyen and Longyearbyen Airport (78°13′32.88″N, 15°36′39.96″E), on the horizontal eastern limb of the Central Basin syncline (hereafter referred to as the Airport Road section).This area was chosen for study as the sub-horizontal bedding (~2–3° dipping to the southwest) means that the lateral continuity of beds, facies associations, and facies successions can be more readily assessed, complementing the vertically-bedded, laterally-limited Festningen section. These sites were chosen because they have been previously well-studied, and therefore already have a robust biostratigraphic framework in place (e.g., Frebold, 1928, Parker, 1967; Vickers et al., 2016; Midtkandal et al., 2016). While the origin of the glendonites (Vickers et al., 2018), and the terrestrial record of the early Aptian ocean anoxic event (OAE1a) have been studied by the authors of this study and others, at these sites (Vickers et al., 2016; Midtkandal et al., 2016), a combined study using the bulk organic $\delta^{13}C$ record to precisely correlate glendonite-bearing successions from across the globe has not been undertaken. Thus, it has not been possible to interpret the significance of the Lower Cretaceous glendonites of Svalbard in a global climatic context.

Facies Analysis

The Festningen and Airport Road sections were logged at 1 m = 2 cm scale, recording grainsize, sedimentary and diagenetic structures (including glendonites and their abundance), paleoflow directions, body and trace fossils. Facies and facies associations were recorded in order to assign environments of deposition and estimate paleobathymetries of the glendonite-bearing horizons.

Carbon Isotope Stratigraphy

Carbon isotope stratigraphy can be used as a useful correlation tool for successions that are biostratigraphically limited (e.g., Kaljo and Martma, 2006), and a number of previous studies have used the organic carbon record to study global carbon isotope excursions (CIEs) in the Early Cretaceous (e.g., Menegatti et al., 1998; Gröcke et al., 1999; Jahren et al., 2001; Ando et al., 2002; Heimhofer et al., 2003; Herrle et al., 2015). These studies, which use either discrete plant fragments or disseminated organic matter from well-dated successions, record a distinct succession of >3 ‰ carbon isotope excursions which are also found in the equivalent inorganic carbonate record (e.g., Weissert and Erba, 2004; Föllmi et al., 2006; Herrle et al., 2015; Price et al., 2016). It is important to use organic matter from the same source as mixing of organic matter (OM) sources can lead to significance bias in the $\delta^{13}C_{org}$ record (e.g., Hunt 1996; Suan et al., 2015). A number of techniques may be used to determine the proportions of marine and terrestrial organic matter, and the thermal maturity. Here, we use palynofacies analysis and gas chromatography–mass spectrometry (GC-MS) to determine the OM source and maturity.

Sampling

The approach of this study is to identify these distinct excursions from the organic record preserved in the Lower Cretaceous succession of Svalbard, and tune the record to the time-calibrated composite global carbon isotope record of the Lower Cretaceous (constructed using data from Weissert and Erba, 2004; Föllmi et al., 2006; Ogg and Hinnov, 2012; Herrle et al., 2015; and Price et al., 2016). To this end, bulk rock samples were collected every 0.5 m, where possible, at the Festningen section (n = 849) and the Airport Road section (n = 279). Samples were taken by excavating the surface rock by up to 30 cm in order to mitigate the effects of surface weathering on subsequent analysis.

$\delta^{13}C_{org}$ Analyses

A total of 617 samples of bulk rock were analyzed for carbon-isotopic composition of the organic carbon within them. Of these, 463 were taken from the Festningen locality and 154 from the section by the Airport Road, Longyearbyen. Samples were ground to a fine powder using an agate mortar and pestle. Powdered samples were decarbonated by placing the sample in a 50 ml polypropylene centrifuge tube and treating with 10% HCl for 1 h until all the carbonate had reacted. The samples were then rinsed with deionized water, centrifuged, and rinsed again until neutrality was reached (following the method of Gröcke et al., 1999). Carbon isotope analysis was performed at the University of Plymouth, UK using an Isoprime isotope ratio mass-spectrometer connected to an Isoprime MicroCube elemental analyzer. Between 1.0 and 3.0 mg of sample were measured into tin capsules for analysis. Carbon isotope ratios are expressed in the internationally accepted per mil (‰) standard notation relative to the Vienna Pee Dee belemnite standard. Instrument calibration was achieved using two international standards, U.S. Geological Survey (USGS) 40 (l-glutamic acid, $\delta^{13}C$ = –26.389 ‰) and USGS 24 (graphite, $\delta^{13}C$ = –16.049 ‰). The mean $\delta^{13}C$ value and the standard deviation on replicate analyses of USGS 40 standard was 26.49 ± 0.08 ‰.

Palynofacies and Analysis of Organic Matter using Gas Chromatography–Mass Spectrometry (GC-MS)

The Lower Cretaceous succession of Svalbard is represented by both marine and terrestrial sedimentary rocks, which may yield organic carbon from different sources. Because marine phytoplankton and terrestrial flora fractionate carbon isotopes differently (Tyson, 1995 and references therein; Hunt, 1996), and the difference between marine and terrestrial organic $\delta^{13}C$ (given the same atmospheric $\delta^{13}C$) may be as great as 12 ‰ (Tyson, 1995), it is necessary to look at $\delta^{13}C_{bulk\ org}$ from broadly the same source, or to assess the degree of mixing between marine and terrestrial carbon through any succession. To do this, palynofacies analysis of the organic matter, and GC-MS analyses of organic extracts (e.g., Tissot and Welte, 1984; Tyson, 1995; Hunt, 1996; Peters et al., 2005) was undertaken.

Additionally, because the succession was subject to intrusion by the Diabasodden Suite, differential thermal alteration of the organic matter might also have modified the $\delta^{13}C_{org}$ record of the organic material. Progressive heating of land-derived organic matter to <450 °C has been shown to alter the mean $\delta^{13}C$ signal to (on average) ~1 ‰ more negative (Jones and Chaloner, 1991; Turney et al., 2006). Therefore, it is important to also assess the thermal maturity of the organic material in order to assess the influence of baking on the secular $\delta^{13}C$ record. Thermal maturity can also be assessed through GC-MS analysis of organic extracts.

For the palynofacies analysis, a total of 20 bulk rock samples from the upper part of the Rurikfjellet Formation in the Festningen section were selected for palynological analysis. Samples were prepared at Paleolab Ltd., Merseyside, UK. All samples were processed following standard palynological preparation procedures (Wood et al., 1996) including treatment for 25 min with HNO_3 to clean them, and sieving at 10 and 5 µm to avoid loss of small palynomorphs. Material was identified as falling into 13 categories (see Supplementary Material Table DR2[1]). A series of non-overlapping traverses across each slide was made, and the particle passing closest to the center of each field of view was counted, until 300 counts were reached.

For the GC-MS analysis, 11 samples of dried crushed rock, from throughout the succession, were accurately weighed into a vial and extracted using a modified Bligh and Dyer extraction. Sediment was extracted with methanol/dichloromethane/phosphate buffer in the ratio 2:1:0.8 (v/v/v) using sonication (10 min). The extraction was repeated three times. The mixture was then centrifuged and the liquid phase decanted, combining extracts and changing the phase ratio to 1:1:0.8. After mixing (vortex, 10 s) and centrifugation (2500 rpm/5 min) the aqueous phase was decanted to waste. The organic layer was washed twice with water before drying by the addition of sodium sulfate, and transferred, with washings, to a pre-weighed vial through a pre-extracted cotton wool plug in a Pasteur pipette. Solvent was removed under a gentle stream of nitrogen to obtain the total organic extract (TOE). The TOE was separated using adsorption chromatography on fully activated silica by transfer of the TOE in a small aliquot of *n*-hexane and dichloromethane onto a pre-conditioned silica column and sequentially eluted with *n*-hexane (F1, "aliphatic") and toluene (F2, "aromatic"). Solvent was removed under a gentle stream of nitrogen from the silica extracts. Fractions were diluted to 1 mg mL^{-1} (or 100 µL where no weight was recorded) with the appropriate solvent for GC and GC-MS analysis.

GC-MS analysis was undertaken by splitless sample injection (1 µL; 250 °C; split/splitless inlet) onto an Agilent DB-5ms (30 m × 0.25 mm × 0.25 µm) column with helium carrier gas (1 mL min^{-1}; constant flow mode). The column was interfaced with an Agilent 5975C Inert XL electron impact and chemical ionization mass selective detector and the Agilent 7890A GC oven was programmed from 40 to 300 °C at 10 °C min^{-1} with a 10 min isothermal hold period. Mass spectra were scanned from m/*z* 50–550.

RESULTS

Facies Analysis

Facies and facies associations identified are provided in Table 1, and the distribution of facies associations shown on Figure 3. The facies associations are: FA1—fluvial/delta channel, FA2—delta plain, FA3—mouth bar, FA4—shoreface, FA5—offshore transition zone, and FA6—open marine shelf (offshore).

Sharp-based marine coarsening-up packages representative of progradation under normal regression are ubiquitous through much of the succession (Fig. 3), but their interpretation as regional, flooding-surface-bound parasequences or as autocyclic bedsets is not possible due to the limited opportunity for regional correlation in this study. The majority of the Rurikfjellet Formation consists of a monotonous aggradational succession of open marine shelf (FA6) siltstone, in which smaller-scale coarsening-up succession cannot be determined. At Festningen, the upper 30 m of the formation passes upwards into a succession of current rippled and hummocky cross-stratified sandstones and heterolithics representing the offshore transition zone (FA5). This transition from FA6 to FA5 represents the first clear evidence for progradation and shallowing in the succession, and is also coincident with the first occurrence of glendonite horizons (Fig. 3). The Festningen Member of the Helvetiafjellet Formation consists of a succession of fluvial/delta distributary channel-fills (FA1) dominated by cross-bedded sandstone. The base of the Festningen Member therefore represents a sequence boundary marked by a basinward facies shift, since mouthbars or a shoreface succession are missing between the Rurikfjellet and Helvetiafjellet formations. At Festningen, the Glitrefjellet Member is aggradational to retrogradational, with a succession of

[1]GSA Data Repository item 2019166, GCMS chromatograms and tables of $\delta^{13}C$ data; palynofacies groups used in this palynofacies analysis; and palynofacies count data, is available at http://www.geosociety.org/datarepository/2019 or by request to editing@geosociety.org.

TABLE 1. FACIES ANALYSIS FOR THE FESTNINGEN AND AIRPORT ROAD SECTIONS, SVALBARD, ARCTIC NORWAY COMBINED

Facies association	Description	Interpretation
FA1: Fluvial or deltaic distributary channel	Sharp, erosively-based successions 5–10 m thick, characterized by: (a) 0.2–0.5 m beds of medium-coarse trough-cross bedded sandstone, with no distinct grainsize profile, or (b) a fining-up succession of a discontinuous basal gravel lag, overlain by structureless or plane-bedded coarse sandstone; trough-cross bedded coarse sandstone; ripple cross laminated fine to medium sandstone; lenticular to flaser bedded heterolithics; and coaly shale. (a) occurs in ~80% of cases. Beds in FA1 are organized into large-scale accretion cross sets that extend through the whole height of the succession (i.e., 5–10 m) and downlap the basal erosion surface (i.e., epsilon cross-bedding of Allen, 1963; or inclined heterolithic stratification (IHS) of Thomas et al., 1987). The inclination of these cross strata are approximately normal to paleoflow indicated by trough-cross bedding. FA1 interstratifies with FA2.	The erosional base to this facies association is indicative of scour-and-fill, and FA1 is interpreted as the product of deposition within channels (e.g., Bridge and Diemer, 1983; Miall, 1985). The presence of IHS perpendicular to paleoflow is indicative of the lateral accretion the inner bank of meandering channels (e.g., Thomas et al., 1987). The height of the IHS (5–10 m) suggests the channels had bankfull depths (given decompaction) of at least 5–10 m (Bridge and Diemer, 1983). Coal-bearing shales capping upper parts of IHS in some FA1 deposits suggests plant colonization of the inner bank sometimes occurred, likely due to discharge fluctuations within the channels. The occurrence lenticular to flaser bedded heterolithics in some successions may suggest a tidal influence (e.g., Dalrymple, 2010). Documented fining-up within the facies association is indicative of lower current velocities on the channel margins (e.g., Thomas et al., 1987). Given the context of this facies association, interstratifying with FA2, in which there is clear evidence for subaerial exposure, but also marine influence, FA1 is interpreted as the deposits of 5–10 m deep fluvial to deltaic distributary channels.
FA2: Delta plain	Interstratified coarsening- and fining-up successions. Coarsening-up successions are typically ~2 m thick, and often display a short (<0.2 m) fining-up succession at the top. They consist of bioturbated (including dinosaur footprints) heterolithics, in which the proportion of sandstone increases upwards, followed by (in varying order and not all always present) beds of asymmetrically rippled sandstone; plane-parallel stratified sandstone; structureless sandstone; and, rarely, gravel conglomerate. Bed thickness increases upwards. The coarsening-up packages are typically capped by interbeds of organic-rich shale or coal, and ripple cross laminated sandstone. Rarely, root horizons extend down by ~0.3 m from the top of the succession. Fining-up successions comprise 1–3 m of sharp, erosively based trough-cross-stratified sandstone which pass upward into asymmetrically rippled sandstone, capped by beds of heterolithic flaser to lenticular siltstone and sandstone, and organic-rich shales. Multiple coarsening-up and fining-up successions stack to form successions up to ≤50 m thick of FA2.	The coarsening-up successions represent the progradation into subaqueous, marine or brackish water of small-scale (at least 2-m-thick, given decompaction) bars at the mouth of small-scale (at least 1–3 m thick, given decompaction) channels, the latter of which are represented by the fining-up successions. The absence of IHS in the fining-up channel deposits (by contrast to FA1), suggests that the channels were short lived, and characterized by rapid incision, and back-filling, rather than lateral accretion. This is characteristic of rapidly avulsing channels at the terminal end of distributary systems (Reading, 1996). The shallow bathymetry of the water, combined with the abundance of plant material and coal clasts in these successions, supports the notion that these were mouth bars deposited on the delta plain. The presence of root horizons, trace fossils left by large terrestrial vertebrates, and organic-rich shales and coals on the tops of the coarsening-up successions with a fining-up cap suggests that these successions represent an episode of a standing body of water filling up to the top, with developments of marshes and mires when shallow enough depths were attained. The presence of marine bioturbation and occurrence of flaser, wavy, or lenticular bedding in the lower part of the mouth bars suggest the receiving standing bodies of water were attached to marine circulation and affected by tidal currents (i.e., interdistributary embayments; Dalrymple, 2010). Altogether FA2 records various gradational depositional environments found on delta plains (interdistributary bays, mires and marshes, minor mouth bars and minor mouth bar channels).
FA3: Storm-influenced shoreface/wave-dominated delta front mouth bar	FA3 is composed of coarsening-up units ~15 m thick, consisting of heterolithics with marine bioturbation (including chondrites and *cosmorhaphe*); massive, structureless medium-coarse sandstone; plane-parallel laminated and trough cross-bedded sandstone. Rarely, the upper 3 m of some units fine-up through structureless medium-coarse sandstone into weakly hummocky cross-stratified sandstone, and rare beds of gravel conglomerate may also be present. Thin, organic-rich shale or coal beds may be present at the top of such successions.	The high proportion of structureless sand, presence of trough cross-bedding and plane-parallel laminations, high organic content (coal-bearing shales and coal beds), and coarsening-up profile displayed by individual packages within FA3 is characteristic of the deposits of mouth bars (e.g., Bhattacharya, 2006, 2010). Mouth bars form when the bedload carried by a fluvial distributary channel is deposited due to deceleration of the flow when it meets a standing body of water (e.g., Elliott, 1986), and the thick, massive sandstones are testimony to this rapid deceleration of flow. The coarsest load is deposited at the immediate river mouth, whereas the finer fraction may be transported further from the river mouth by the decelerating jet. The coarsening-up profile represents the progradation of the mouth bar. The ~15 m thickness of the mouth bar coarsening-up packages is characteristic of delta-front mouth bars which were prograding into water at least this deep. The context of FA3, overlying clearly marine deposits of FA4, the presence of marine bioturbation, indicates that the mouth bars were prograding into open marine waters. The presence of some weakly hummocky cross stratified beds suggests the mouth bar deposits were reworked by wave and storm currents, although the predominance of evidence for unidirectional flow indicates a proximity to the fluvial outflow, and high depositional rates, which prevented much reworking by waves.
FA4: Distal storm-influenced shoreface	FA5 is composed of coarsening-up successions of sand-dominated heterolithics; current cross-laminated silty fine sandstone; amalgamated hummocky cross-stratified sandstone beds; cross-bedded coarse sandstone (rarely glauconitic); plane-parallel laminated sandstone; rare intensely bioturbated structureless sandstone; organic-rich shales; and coal, not all of which are present in each succession. FA4 successions may be between 2 and 15 m thick, shorter successions consisting only of bioturbated heterolithics, wavy, silty fine sandstone and hummocky cross stratified (HCS) sandstone.	These successions are interpreted as shoreface deposits. Hummocky cross-stratified sandstones interbedded with siltstones are indicative of intermittent storm re-working and suspension settling, characteristic of the lower shoreface. The passage upward through amalgamated hummocky cross-stratified beds is indicative of intense storm-wave reworking, and the upper cross-laminated and trough cross bedded sandstones were the product of ripples and dunes formed by combined flows with a strong unidirectional component, and characteristic of the upper shoreface (e.g., Plint, 2010). Shorter successions lacking large-scale cross-bedding and plane-parallel laminated sandstones are interpreted as lower shoreface successions, close to the lower shoreface-offshore transition boundary. The presence of glauconite in the cross-bedded sands suggests that at times sediment accumulation rates were very low.

(*continued*)

TABLE 1. FACIES ANALYSIS FOR THE FESTNINGEN AND AIRPORT ROAD SECTIONS, SVALBARD, ARCTIC NORWAY COMBINED (*continued*)

Facies association	Description	Interpretation
FA5: Offshore transition zone	FA5 is composed of 2–12-m-thick coarsening-upward successions, laterally extensive over tens to hundreds of meters. FA5 consists of "spaced-laminated" siltstone at the base, passing upward through bioturbated heterolithic sandstone and siltstone. The coarsening-upwards successions are characterized by the introduction of symmetrically and asymmetrically rippled, and HCS, sandstone beds, which interstratify with "spaced-laminated" siltstone with increasing abundance upwards, and become thicker. Beds of plane-parallel-laminated sandstones, which grade into hummocky-cross stratified sandstone or asymmetrically rippled sandstone, are also found towards the top of these coarsening-up successions. Discontinuous fossiliferous lags also occur, containing marine biota such as belemnites, and glendonite horizons. In the coarsest, most sand-dominated examples of this facies association, ≤3 m long x ≤1.5 m deep scours occur within these coarsening-up packages, which are filled with HCS or plane-parallel-laminated sandstone. Paleocurrent measurements in FA5 are unimodal or bimodal. Unimodal paleocurrents record mean flow direction to the southeast.	The coarsening-up successions were deposited in an environment with alternating episodes of vertical suspension settling of silt, and the input of fine sand via unidirectional (gravity) currents. This was periodically interrupted by storm-generated oscillatory currents of varying strength; sometimes scouring the sediment surface, then depositing sand in the upper flow regime under powerful combined flows (C6). As currents waned, sediment settling under oscillatory flow produced HCS and symmetrically rippled sands with ever-decreasing current flow velocities (e.g., Plint, 2010). In combination with the presence of belemnites, the evidence is indicative of deposition in the marine offshore transition zone setting, between the fairweather and storm wave bases. Settling from suspension and weak gravity currents below fairweather wave base were periodically interrupted by storm reworking of sands.
FA6: Open marine shelf (offshore)	FA6 consists of successions exceeding 400 m thick, gradually coarsening-up successions of paper and "spaced" laminated claystones and siltstones, heterolithic silts and fine sands showing current cross-lamination. Up succession, discontinuous, 0.1–0.2-m-thick carbonate beds give way to horizons of carbonate lenses and cannon-ball concretions and, less commonly, glendonite horizons. Marine fossils such as belemnites and ammonites are rarely present.	The great thickness of FA6 successions, apparent great lateral continuity, fine grain size, limited bioturbation, and rare open marine fossils (including a single ammonite), absence of oscillatory current bed-forms but presence of current-ripples, together suggest that FA6 represents deposition via hemipelagic suspension settling and rare low concentration density currents in an open marine shelf environment, below the storm wave base.

delta plain (FA2) heterolithics, overlain by an 8-m-thick erosional-based distributary channel fill (FA1) sandbody and 7 m of wave-influenced delta-front mouth bar heterolithics and sandstone. The retrogradational motif is continued in the Carolinefjellet Formation at Festningen and the Airport Road sections. Current rippled and hummocky-cross stratified offshore transition zone (FA5) heterolithics and shoreface (FA4) sandstones with hummocky cross-stratification, plane-parallel lamination, and trough-cross bedding, in the lower 90 m of the formation pass upward into open marine shelf (FA6) laminated siltstone, and rippled heterolithics to thin hummocky cross-stratified beds of the offshore transition zone (FA5). The return to more distal, marine (shoreface-offshore transition zone) sediments also marks a return to glendonite-bearing horizons (Fig. 3). More details of the host lithology for the glendonites, and the form of the glendonites (e.g., rosette, or inside concretions), and their hypothesized growth and preservation can be found in Vickers et al. (2018).

Carbon Isotope Stratigraphy

The full suite of $\delta^{13}C_{bulk\ org}$ analyses is provided in Supplementary Table DR1, and the stratigraphic distribution of each result is shown in Figure 3. The mean value for all the bulk rock samples is –24.56 ‰, and the standard deviation is 1.18 ‰, with an overall variation of 7.11 ‰. Our data compare closely with numerous other studies of the Early Cretaceous carbon isotope record (e.g., Gröcke et al., 1999; Ando et al., 2002; Heimhofer et al., 2003; Herrle et al., 2015), showing the same major (>3 ‰) excursions associated with the OAE1a CIE and similar increasing and decreasing trends (discussed in detail in the following section).

The full suite of results from the palynofacies analysis is provided in Supplementary material Table DR3. A total of 98.2% of the analyzed particles were terrestrial in origin, with 85% being terrestrial phytoclasts and 15% palynomorphs (spores, pollen, prasinophycean algae, and dinoflagellate cysts). There is a negligible (<0.5%) amount of amorphous organic matter (AOM) in the analyzed samples. The organic material in the samples generally fall into palynofacies field III on a ternary AOM-phytoclast-palynomorph kerogen plot (Fig. 4A) (proximal/heterolithic oxic shelf; Tyson, 1995), with some samples falling into field I (highly proximal shelf or basin). These results indicate an overwhelming (but not complete) terrestrial source for these palynofacies-analyzed samples between 300 and 450 m.

A cross-plot of pristane/nC_{17} and phytane/nC_{18} ratios (Fig. 4B) indicated that organic matter in all sediments analyzed had a terrestrial (possibly lacustrine) source subject to oxidative conditions. The *n*-alkane $\Sigma nC_{21-}/\Sigma nC_{21+}$ ratio was generally <1 (Table 2), with longer chain n-alkanes (which are more usual from terrestrial sources) dominating, with values >1 at 400–506.5 m indicating algal/bacterial input. C_{27} (all sources), C_{28} (marine or limnic algal origin), and C_{30} (marine algal origin) steranes were not detected in any of the sediment extract chromatograms (*m/z* 217 plus m/z 372, 386, and 414, respectively), while weak signals for the C_{29} sterane (*m/z* 217, 400) terrestrial plant marker was detected in sediments extracts above 506.5 m (data not shown). There was little variance in the Carbon Preference Index (CPI) value throughout the sediment profile (1.0–1.1; Table 2) indicating full thermal maturity throughout the sequence (Tissot and Welte, 1984). The MPI-1 ratio varied between 0.6–0.9 and calculated vitrinite reflectance values (Rc; Table 2; Radke and Welte, 1983) indicate mature sediments within the oil window or at the more mature end of wet gas generation. The presence of *n*-alkanes ranging from around C_{15}–C_{35} in the "aliphatic" (F1) extracts of all samples (Supplementary Material Fig. DR1) indicates that the samples have undergone slight to moderate biodegradation. This was supported by the lack of a pronounced "unresolved complex mixture" in these chromatograms (Supplementary Material Fig. DR1) and the presence of phenanthrene compounds in chromatograms of the "aromatic" (F2) extracts (Supplementary Material DR1).

Hence, the origin of the organic matter, and thermally induced chemical alteration of the organic material for those samples analyzed does not appear to have significantly impacted

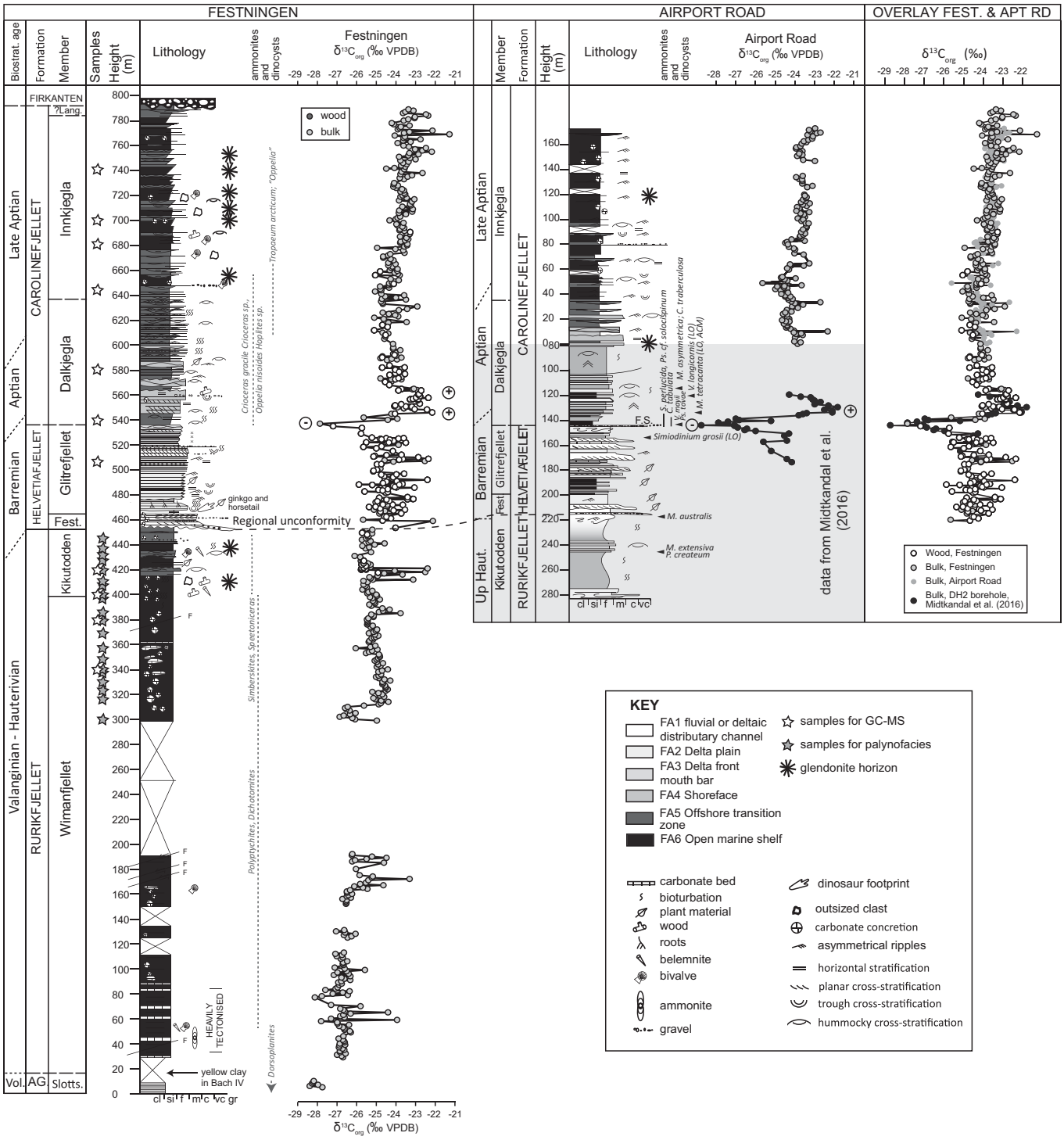

Figure 3. Correlation of sedimentary logs and $\delta^{13}C_{bulk\ org}$ for the Festningen section with the Airport Road section and DH-1 borehole, Spitsbergen, Norway. Festningen log between 395 and 705 m adapted from Vickers et al. (2016 and 2018). Facies associations denoted by different colors on the logs (see key). The $\delta^{13}C_{bulk\ org}$ data (this study) is shown in gray circles; δ13Cwood data (Vickers et al., 2016) in brown circles; $\delta^{13}C_{bulk}$ data (Midtkandal et al., 2016) from the DH-1 borehole in red circles. Existing biostratigraphic age model for each site is also shown. Occurrences of ammonites at Festningen (Frebold, 1928; Parker 1967) and dinoflagellate cysts from the Longyearbyen borehole (Midtkandal et al., 2016) are also shown next to the logs. LO—last occurrence, ACM—acme (mass abundance). Yellow stars indicate height at which samples were taken for gas chromatography–mass spectrometry (GC-MS) analyses; red stars indicate horizons where samples were taken for palynofacies analysis. AG.—Agardhfjellet Formation; Fest.—Festningen Member; Slotts.—Slottsmøya Member; Lang.—Langstakken Member, Up. Haut.—Upper Hauterivian; Vol.—Volgian; Biostrat.—Biostratigraphic; F.S.—flooding surface; F—fault; VPDB—Vienna Pee Dee belemnite. cl—clay; si—silt; f—fine; m—medium; c—coarse; vc—very coarse.

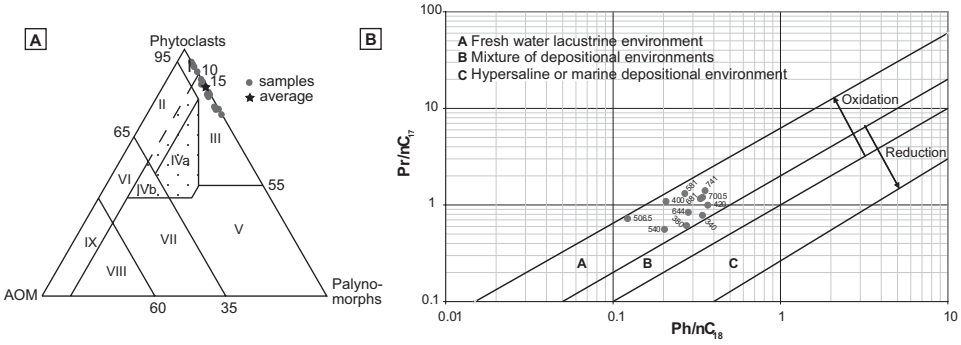

Figure 4. (A) Ternary amorphous organic matter (AOM)-phytoclast-palynomorph kerogen plot displaying the palynofacies data collected from Festningen, Spitsbergen, Norway. Palynofacies fields as identified in Tyson (1995). The palynofacies data fall into field III (heterolithic oxic shelf a.k.a. "proximal shelf"; Tyson, 1995) and field I (highly proximal shelf or basin). (B) Cross plot of phytane/nC$_{18}$ and pristane/nC$_{17}$ ratios indicating source of sedimentary organic matter.

TABLE 2. GRAVIMETRIC RECOVERY OF TOTAL ORGANIC EXTRACT (TOE) FROM SEDIMENTS FROM FESTNINGEN AND TOE "ALIPHATIC" (F1) AND "AROMATIC" (F2) FRACTIONS OBTAINED FROM ADSORPTION CHROMATOGRAPHY ON SILICA

Sample	TOE		"aliphatic" (ALI) (F1)	"aromatic" (ARO) (F2)	ALI/ARO	Uncharacterized		Pr/nC$_{17}$	Ph/nC$_{18}$	Pr/Ph	MPI-1	Rc	Rc	ΣnC$_{21-}$/ ΣnC$_{21+}$	CPI
	mg	µg g^{-1}	µg g^{-1}	µg g^{-1}		µg g^{-1}	%								
741	0.6	101	50	17	3	34	33	1.4	0.4	3.1	0.6	0.8	1.9	0.8	1.1
700.5	0.4	66	<8	<8	1	56	85	1.2	0.3	2.5	0.8	0.9	1.8	0.7	1.1
681	0.4	80	20	<8	4	55	69	1.2	0.3	2.2	0.6	0.8	1.9	0.9	1.0
644	0.5	77	<8	<8	1	67	87	0.8	0.3	1.9	0.7	0.8	1.9	0.6	1.1
581	0.9	173	39	77	1	58	33	1.3	0.3	3.3	0.8	0.9	1.8	0.6	1.1
540	0.6	113	94	57	2	–38	–33	0.6	0.2	1.9	0.7	0.8	1.9	0.6	1.1
506.5	0.9	178	39	20	2	118	67	0.7	0.1	4.3	0.6	0.7	2.0	1.0	1.1
420	0.2	29	<8	<8	1	19	66	1.0	0.4	2.1	0.9	0.9	1.8	1.3	1.0
400	0.5	85	34	51	1	0	0	1.1	0.2	2.6	0.7	0.8	1.9	1.0	1.0
380	3.1	547	<8	<8	1	537	98	0.6	0.3	1.7	0.7	0.8	1.9	0.8	1.0
340	0.4	67	17	<8	3	45	67	0.8	0.3	1.3	0.7	0.8	1.9	0.6	1.0

Notes: Pr—pristane; Ph—phytane; MPI—Methylphenanthrene index; Rc—vitrinite reflectance; CPI—carbon preference index.

the $\delta^{13}C_{bulk\ org}$ composition of the preserved organic material. Likewise, Koevoets et al. (2016) and Midtkandal et al. (2016) comparing $\delta^{13}C_{org}$ isotopes and Rock Eval parameters from the Upper Jurassic Agardhfjellet Formation and Barremian to Aptian Helvetiafjellet to Carolinefjellet Formations, respectively, suggest only a limited influence of organic matter source, diagenesis, thermal maturation, and weathering on the $\delta^{13}C_{org}$ values. The Rock Eval data from Midtkandal et al. (2016) spans the critical interval containing the OAE1a CIE in the DH2 borehole (directly underlying the Airport Road section) and, as they show no significant correlation with $\delta^{13}C$, thus compliment our Rock Eval and palynofacies data from the Rurikfjellet Formation and corroborate the validity of using our composite $\delta^{13}C_{org}$ curve for correlation with other localities. The $\delta^{13}C_{bulk\ org}$ data are shown to be closely aligned, particularly clearly across the negative and positive CIEs in the Glitrefjellet and Dalkjegla members, with $\delta^{13}C$ measurements of fossil wood from Vickers et al. (2016) from the Festningen section (Fig. 3), and $\delta^{13}C_{bulk\ org}$ data from the DH-1 borehole through stratigraphy that is continuous with the Airport section (Fig. 3), of Midtkandal et al. (2016).

DISCUSSION

Paleobathymetry of Lower Cretaceous Glendonites of Svalbard

Natural conditions that promote ikaite formation at the expense of the anhydrous polymorphs of $CaCO_3$ (i.e., calcite and aragonite) require the presence of inhibitors of calcite and aragonite growth and promotion of ikaite growth. As ikaite increases stability with decreasing temperature (while the anyhydrous polymorphs decrease stability with temperature decrease; Spielhagen and Tripati, 2009; Purgstaller et al., 2017; Stockmann et al., 2018), low temperatures are expected, and found, at natural ikaite precipitation sites (e.g., Jansen et al., 1987; Bischoff et al., 1993; Buchardt et al., 2001; Selleck et al., 2007; Dieckmann et al., 2008; Zhou et al., 2015; fig. 8 in Purgstaller et al., 2017). With increasing concentrations of strong chemical inhibitors of calcite and aragonite growth, such as magnesium, sulfate, or phosphate ions, hyperalkalinity, and supersaturation with respect to ikaite, temperatures at which ikaite can grow may be higher (e.g., Nielsen et al.,. 2016; Field et al., 2017; Stockmann et al., 2018), but there appears to be an upper limit of 12–15 °C as shown by laboratory experiments (e.g., Brooks et al., 1950; Purgstaller et al., 2017; Stockmann et al., 2018). The conditions under which ikaite precipitated under these warmer temperatures do not appear to be representative of the conditions found in the ikaite formation zone in the modern marine sedimentary realm (Zhou et al., 2015), and in no known natural marine sedimentary settings has ikaite been reported forming at above 7 °C (e.g., Suess et al., 1982; Schubert et al., 1997; Greinert and Derkachev, 2004; Zhou et al., 2015; fig. 8 in Purgstaller et al., 2017). Two biogeochemical processes are thought to create the chemical conditions necessary for ikaite growth; organotrophic and methanotrophic sulfate reduction (e.g., Teichert and Luppold, 2013), and the responsible process is thought to be distinguishable by the $\delta^{13}C$ values of the glendonite (e.g., Greinert and Derkachev, 2004; Teichert and Luppold, 2013; Morales et al., 2017; Vickers et al., 2018). The $\delta^{13}C_{carbonate}$ data for the glendonites in this study are within the range expected for an organic matter source (–13.3 ‰ to –30.9 ‰, Vickers et al., 2018; Morales et al., 2017), and there is no other evidence (chemical or sedimentological, e.g., methane seep carbonates) that methane

seepage was occurring in the sediments in which the Lower Cretaceous glendonites of Svalbard are found.

Based on the facies analysis carried out in this study, it is demonstrated that the glendonites formed in sediments that were remarkably similar to the marine sedimentary settings in which ikaite may be found growing today (Zhou et al., 2015). Temperature conditions for all modern marine sedimentary ikaite is below 7 °C (often closer to 0 °C), and thus the presence of glendonites in these oxic, offshore transition zone to open marine shelf sediments of this study argue for temperatures below 7 °C in the ikaite formation zone (Zhou et al., 2015).

In the modern day, ocean temperatures are below 7 °C in near surface bathymetries at latitudes typically >64°N and >45°S and can occur at less than 750 m depth in equatorial regions. Ikaite has been shown to grow naturally at equatorial latitudes; for example in the Zaire submarine fan, off the African passive margin at depths of over 3000 m (Jansen et al., 1987; Zabel and Schulz, 2001). Ocean floor successions of this great bathymetry are rarely preserved at outcrop, except fragments of obducted lithosphere, but submarine fan and shelf margin slope successions, which in the modern day occur at depths >200 m (e.g., Patruno et al., 2015) are abundant at outcrop. Therefore, when arguing for the occurrence of glendonites as an indicator of a "cold" ocean (for example, capable of supporting small polar ice-caps), it is important to consider the paleo-water depth, as well as the paleo-latitude, at which the ikaite originally formed. Mesozoic glendonites are abundantly documented from paleo-high-latitude sites (e.g., De Lurio and Frakes, 1999; Price and Nunn, 2010; Grasby et al., 2017 and references therein, Morales et al., 2017; Rogov et al., 2017 and references therein), and have been used to argue for so-called Cretaceous "cold-snaps" (e.g., Kemper, 1987). However many of these studies do not record, or are ambiguous about the depositional environment of documented glendonites (e.g., Grasby et al., 2017; Morales et al., 2017; Rogov et al., 2017), and estimation of the water depth at which they formed is difficult because insufficient sedimentological and facies information is provided by those studies.

The glendonites of Lower Cretaceous Svalbard occur in sediments deposited in the open marine shelf and offshore transition zone (Fig. 3), and in one instance even into the shoreface environment. The offshore transition zone is interpreted as occurring between the storm and the fair weather wave bases (i.e., above the depth of agitation of the sea floor by the waves generated during the largest storms, or tsunami; Table 1). In the modern day, this depth may be as much as 110 m along shelf edge coastlines facing the open ocean (e.g., passive margins; Plint, 2010; Peters and Loss, 2012), but less than 70 m on broad epicontinental shelves (Plint, 2010). However, in the Cretaceous, increased storm intensity (Ito et al., 2001) may have resulted in a deeper storm wave base (SWB). By comparison, marine sedimentary glendonites in this study are generally found in the offshore transition zone, above the SWB (in one instance even found in sediments as shallow as shoreface; Fig. 3). This may be a reflection of the paleo-ocean temperatures remaining consistently below the threshold for ikaite precipitation (e.g., <7 °C) at these shallow bathymetries (likely <100 m) at all times.

In the present day ocean the mechanisms for producing cold temperatures in coastal waters are either from local heat exchange with the atmosphere (such as in present day high latitudes), transport of colder water by coastal currents, or from the upwelling of cold water along continental margins, such as on the coast of South America/Africa. Upwelling of cold water requires two conditions; persistent alongshore winds and a pool of cold water at depth from which to draw (Stewart, 2008). The aspect and paleogeography of Svalbard during the Early Cretaceous (Fig. 1) make upwelling conditions unlikely, as GCM simulations have suggested (e.g., Price et al., 1995; Brady et al., 1998; Haupt and Seidov, 2001); the bathymetry is relatively shallow across a wide area ruling out a source of trapped cold water to draw from and is semi enclosed reducing the likelihood of appropriate wind conditions.

If we discount upwelling of cold waters as unlikely, this leaves the drivers of cold coastal temperatures as the local heat exchange and coastal currents. Coastal currents are most often buoyancy driven from riverine input (the temperature of which reflects local atmospheric conditions, e.g., Webb et al., 2003; Yang and Peterson, 2017) and, unlike upwelling which can introduce pristine cold water into warm environments, coastal currents are subject to mixing from bottom friction, tides, and storms reducing their temperature difference from the surrounding sea (Simpson and Sharples, 2012). The glendonites were all found above the SWB, indicating areas of significant mixing at least during storm periods, and thus suggest the glendonites are representative of a general cold water and air temperatures around this latitude during certain periods, a conclusion supported by the occurrence of glendonite horizons in the Canadian Arctic and Siberia (see following section). Given the requirement for meridional temperature gradients to balance the global heat budget (e.g., Bice and Norris, 2002; Fluteau et al., 2007; Stewart, 2008; Boyer et al., 2013), these temperatures are consistent with polar temperatures capable of supporting a north polar ice cap.

Global Correlation of Glendonite Occurrence in the Lower Cretaceous

The high fidelity $\delta^{13}C_{org}$ curve generated in this study is shown on Figure 5, together with the global composite $\delta^{13}C_{carbonate}$ curve for the Lower Cretaceous. The a priori correlation between the two curves is the in-place biostratigraphic framework (Fig. 3; fig. 2, p. 4 from Vickers et al., 2016 and references therein). At Festningen, occurrences of Valanginian ammonites (*Polyptychtes, Dichomites, Temnoptychites*) have been reported from throughout the Wimanfjellet Member (Frebold, 1928; Parker, 1967; Ershova, 1983), and Hauterivian ammonites from the Kikutodden Member (*Simberskites, Speetoniceras*; Parker, 1967; Ershova, 1983). However, more recent palynological studies from other localities in central Spitsbergen, including from the Longyearbyen area, extend the age of the Wimanfjellet Member into the Hauterivian (by presence of dinocysts of the *Rhynchodiniopsis aptiana* zone, Århus, 1992), and that Kikutodden Member into the Barremian (using the presence of *Muderongia australis; Gardodinium ordinale; ?Nyktericysta pannos; Pseudoceratium polymorphum*; Grøsfjeld, 1992; Midtkandal et al., 2016). Biostratigraphy is lacking from the Helvetiafjellet Formation, across Spitsbergen, owing to the terrestrial and paralic nature of the facies preserved here (e.g., Mørk et al., 1999). The overlying marine Carolinefjellet Formation is constrained to the Aptian, at Festningen, by the presence of *Crioceras sp., Oppelia nisoides, Hoplites sp.* (in the Dalkjegla Member; Frebold, 1928), and upper Aptian *Tropaeum arcticum* (Dalkjegla-Innkjegla members; Sokolov and Bodylevsky, 1931; Frebold and Stoll 1937; Ershova, 1983). Furthermore, upper Aptian dinocysts (*Caligodinium aceras; Gonyaulacysta sp. I; Murderongia asymmetrica; M. mcwhaei; Oligosphaeridium albertense; O. totum; Tenua brevispinosa*) have been described from the Inkkjegla Member near Adventdalen and the East coast (Hiorthfjellet and Agardhfjellet; Thusu, 1978). There are no descriptions of Albian faunas at Festningen, and younger members of the Carolinefjellet Formation are absent here (Nagy, 1970).

Within this existing framework, discrete isotopic excursions with distinctive directions of change, magnitudes, and shapes can be correlated to similar excursions seen in other

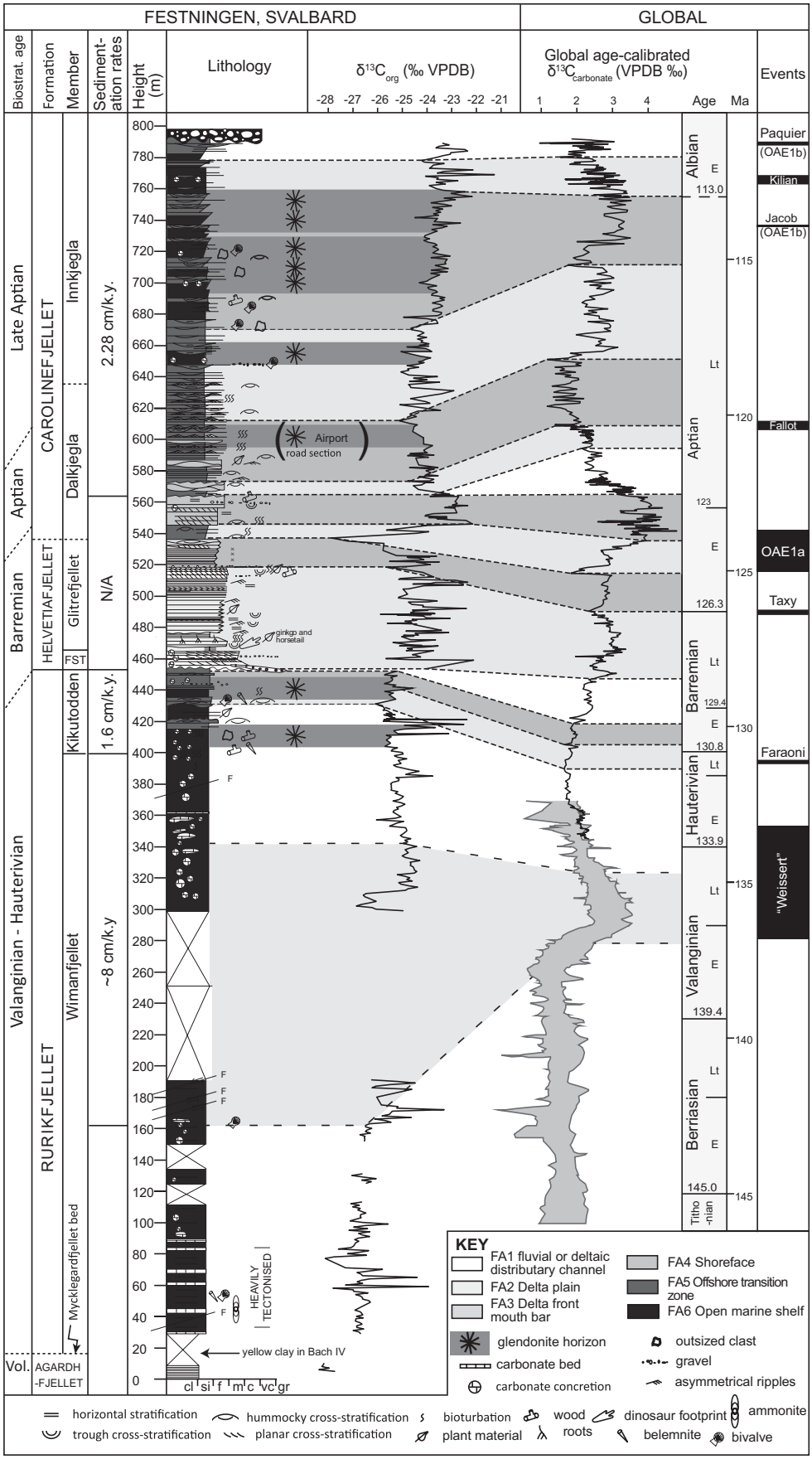
FESTNINGEN, SVALBARD
GLOBAL
Biostrat. age
Formation
Member
Sediment-ation rates
Height (m)
Lithology
δ13Corg (‰ VPDB)
Global age-calibrated δ13Ccarbonate (VPDB ‰)
Age
Ma
Events
Late Aptian
Aptian
Barremian
Valanginian - Hauterivian
CAROLINEFJELLET
HELVETIAFJELLET
RURIKFJELLET
Innkjegla
Dalkjegla
Glitrefjellet
FST
Kikutodden
Wimanfjellet
Myckelegardfjellet bed
2.28 cm/k.y.
N/A
1.6 cm/k.y.
~8 cm/k.y
Vol.
AGARDH -FJELLET
Airport road section
ginkgo and horsetail
HEAVILY TECTONISED
yellow clay in Bach IV
Albian
Aptian
Barremian
Hauterivian
Valanginian
Berriasian
Tithonian
Paquier
(OAE1b)
Kilian
Jacob
(OAE1b)
Fallot
OAE1a
Taxy
Faraoni
"Weissert"
KEY
FA1 fluvial or deltaic distributary channel
FA2 Delta plain
FA3 Delta front mouth bar
FA4 Shoreface
FA5 Offshore transition zone
FA6 Open marine shelf
glendonite horizon
carbonate bed
carbonate concretion
outsized clast
gravel
asymmetrical ripples
horizontal stratification
trough cross-stratification
hummocky cross-stratification
planar cross-stratification
bioturbation
plant material
wood
roots
dinosaur footprint
belemnite
ammonite
bivalve

Figure 5. Summary log of the Festningen section, Spitsbergen, Norway, with horizons containing glendonites highlight in blue. Biostratigraphic (Biostrat.) age for the succession (for references see Geological Setting and Fig. 3) is shown on the left. Calculated uncompacted sedimentation rates shown to the left of the lithostratigraphy. $\delta^{13}C_{org}$ (both wood and bulk) from the Festningen section is correlated to the composite global $\delta^{13}C$ curve from carbonate records. Composite $\delta^{13}C_{carbonate}$ curve constructed from Weissert and Erba (2004), Föllmi et al. (2006), Herrle et al. (2015), and Price et al. (2016); tuned to Ogg and Hinnov (2012). Dark- and light-gray areas indicate correlative intervals. Global cool episodes indicated by blue shaded area on timescale; warming episodes indicated in red shaded area on timescale. Position of Aptian ocean anoxic event (OAE1a) relative to the carbon-isotope records also displayed. FST—Festningen Member. Timing of High Arctic Large Igneous Province volcanism on Svalbard from Nejbert et al. (2011). VPDB—Vienne Pee Dee belemnite; E—early; Lt—late; Vol.—Volgian. cl—clay; si—silt; f—fine; m—medium; c—coarse; vc—very coarse; gr—gravel.

Arctic organic records (Herrle et al., 2015; Fig. 6) and the global $\delta^{13}C_{carb}$ curve for the Tithonian to Albian (Fig. 5). This allows for the finer tuning of the correlation of the glendonite horizons. Clearly recognizable in both the regional correlation with the Canadian Arctic $\delta^{13}C_{org}$ record (Herrle et al., 2015) and the global carbonate record are (1) the distinctive negative CIE of OAE1a and the double positive in the recovery of this event; (2) the inflection of the curves in the upper Hauterivian; and (3) the distinctive negative trend through the lower upper Aptian. The correlation between the Festningen section $\delta^{13}C_{org}$ data and the global $\delta^{13}C_{carbonate}$ curve become less certain in the lowermost 400 m and in the uppermost ~150 m. In the uppermost Aptian there is an absence of large, significant, correlatable global $\delta^{13}C$ excursions, and longer-term trends in the global $\delta^{13}C_{carbonate}$ curve are not apparent in the Festningen $\delta^{13}C_{org}$ curve.

Using the chemostratigraphic framework developed in this study, glendonite-bearing intervals in the Lower Cretaceous of Svalbard can be correlated with those of the Canadian Arctic (Fig. 6), and other Lower Cretaceous glendonite-bearing sites in both Southern and Northern hemispheres, using our correlation to the global carbonate curve (Figs. 5 and 7), as well as to major hypothesized episodes of global cooling derived from alternative, independent proxies (Fig. 7; e.g., Pucéat et al., 2003; Erba et al., 2004; Harland et al., 2007; McArthur et al., 2007; Mutterlose et al., 2009; McAnena et al., 2013; Price and Passey, 2013; Bodin et al., 2015). In this study, glendonites deposited in bathymetries <100 m water occur in the Kikutodden Member of the Rurikfjellet Formation, which is Hauterivian to earliest Barremian in age, the middle Dalkjegla Member and throughout the Innkjegla Member of the Carolinefjellet Formation which date from the mid to latest Aptian (Figs. 5 and 7).

Hauterivian to earliest Barremian glendonites of Svalbard post-date major occurrences of glendonites from Russia and Arctic Canada that are mainly late Berriasian to earliest Hauterivian in age, but are possibly synchronous with more poorly dated glendonites from Alaska (Fig. 7). A major cooling event has been proposed for the late Valanginian to early Hauterivian (Bodin et al., 2015), whereby the positive carbon isotope excursion of the "Weissert" CIE has been linked to increased organic carbon burial and consequent increased burial of atmospheric CO_2. The onset of cooling is proposed as coinciding with peak $\delta^{13}C$ values, and is followed by an interval waning of $\delta^{13}C$ values (Erba et al., 2004; Weissert and Erba, 2004; Föllmi et al., 2006). Evidence for cooling is based on the occurrences of tillite and dropstones (Frakes et al., 1995) in sediments of Valanginian and Hauterivian age at a number of places around the globe, paleontological evidence coming from the distribution patterns of calcareous nannofossils (Mutterlose and Kessels, 2000) and the occurrence of cool water-indicating biomarkers (steryl ethers) in claystones of Valanginian age from the Shatsky Rise in the northwest Pacific (Brassell, 2009). Supposed evidence for polar ice at this time is a trend toward positive oxygen isotope values (~lower temperatures) in the $\delta^{18}O$ record of fish teeth enamels (Pucéat et al., 2003), and belemnites (Price and Mutterlose, 2004). Meissner et al. (2015) suggest the $\delta^{18}O$ of belemnites in the late Valanginian to early Hauterivian indicate a cooling of ~4 °C in the southern Boreal Realm and 2 °C in the Arctic Boreal Realm. Although a large number of glendonite occurrences are coincident with the "Weissert Event" CIE (in the Canadian Arctic and Russia; Rogov et al., 2017 and references therein; Grasby et al., 2017 and references therein), the ages of glendonites from this study, as well as those from Northern Russia, Greenland, and Alaska (Fig. 7), argue for a more prolonged cooling, beginning in the late Berriasian, and ending in the early Barremian (at least 8.5 m.y. using the timescale of Ogg and Hinnov, 2012). The initiation of this cooling pre-dates the "Weissert Event" by more than 4 m.y., and continues for a further ~2.5 m.y. after the event (Ogg and Hinnov, 2012). This indicates that the "Weissert Event" CIE and cooling are not mechanistically linked, as has previously been proposed (e.g., Erba et al., 2004; Martinez et al., 2015). This has previously been suggested by other studies, e.g., Lunt et al. (2016), who show that changes in continental configuration can change global circulation and heat transfer patterns on a scale large enough to drive global warming or cooling, independent of atmospheric CO_2 levels.

Glendonites are missing from the upper Barremian to lower Aptian of Svalbard, but much of this time was represented by uplift of the pan-Arctic region (e.g., Gjelberg and Steel, 1995; Galloway et al., 2013; Rogov et al., 2017), hiatus or deposition of terrestrial successions, which do not promote ikaite growth. Glendonites of this age are also unknown in marine successions of NE Russia and Australia (regions characterized by abundant upper Aptian glendonites), so their absence may support evidence for warmth during this period (e.g., Mutterlose et al., 2010; Bodin et al., 2015).

Finally, late Aptian glendonites of Svalbard are synchronous with a major interval of glendonites from Arctic Canada (Fig. 6; Herrle et al., 2015; Grasby et al., 2017), Greenland (Hovikoski et al., 2018), and possibly the Eromanga Basin (Fig. 7; Australia; De Lurio and Frakes, 1999) of the Southern Hemisphere (Figs. 1A and 7). Cooling is proposed for the late Aptian, with evidence coming from belemnite $\delta^{18}O$ records (e.g., Bodin et al., 2015, <4 °C cooling), TEX_{86} sea surface temperature reconstructions (McAnena et al., 2013, ~5 °C cooling), changes in calcareous nannofossil assemblages (Vocontian Basin, Tethys; e.g., Herrle and Mutterlose, 2003) and changes in floral assemblages in the polar regions (Francis and Poole, 2002; Harland et al., 2007). More equivocal evidence for late Aptian cooling (enough to allow the growth of small polar ice-caps) comes from sea-level falls (e.g., Maurer et al., 2013; Millán et al., 2014) and interpreted "glacial dropstones" (e.g., Dalland, 1977; Frakes et al., 1995; Rodríguez-López et al., 2016). Our bathymetrically constrained glendonites lend strong support to the hypothesis of late Aptian cooling, with temperatures low enough for small ice-cap development at the poles.

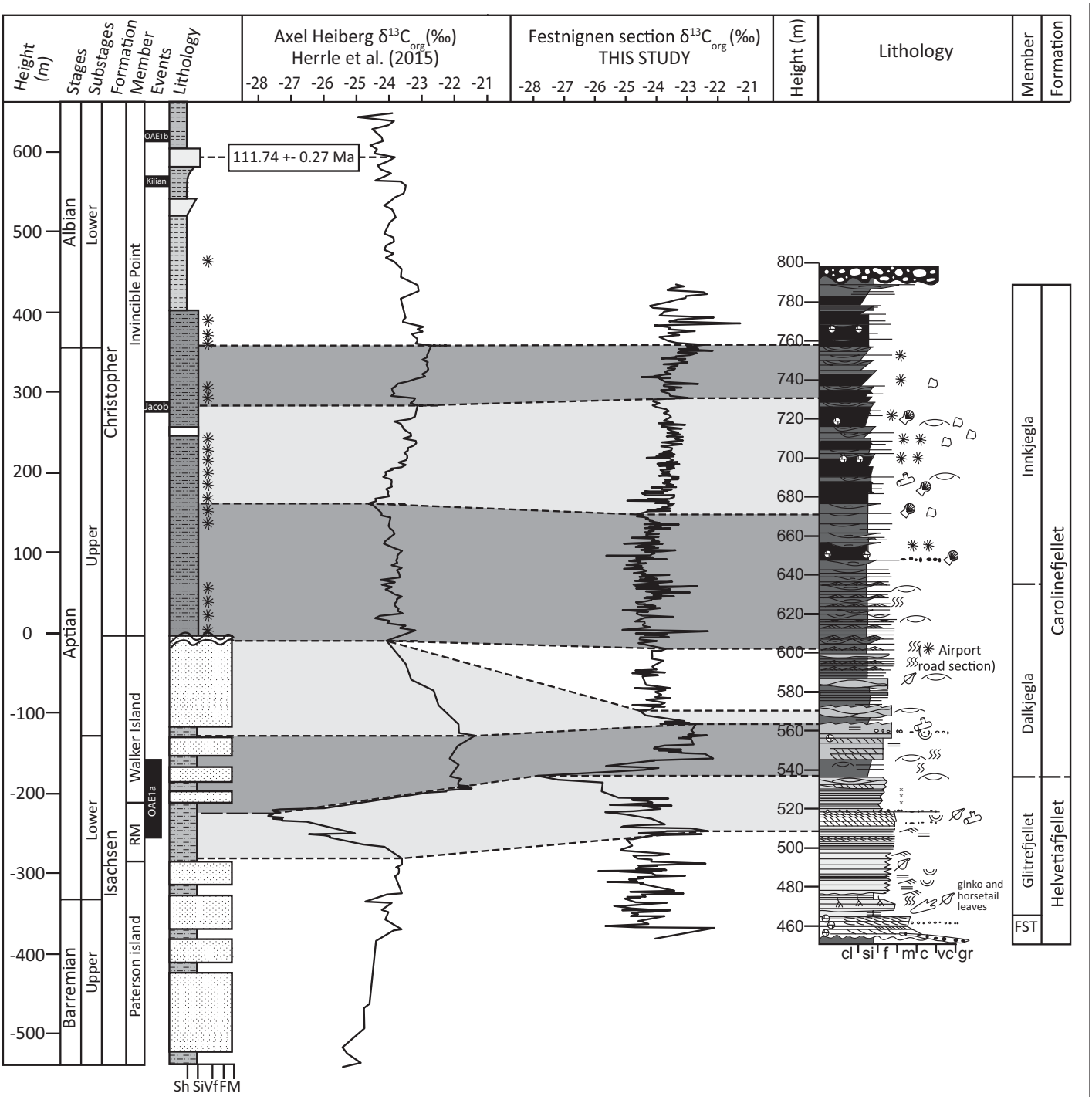

Figure 6. Correlation of $\delta^{13}C_{org}$ data from this study with that for the Barremian–Aptian deposits on Axel Heiberg, Canadian Arctic (Herrle et al., 2015). The log and age constrains for Axel Heiberg are as published in Herrle et al. (2015). FST—Festningen Member. Sh—shale; Si—silt; Vf—very fine; F—fine; M—medium; si—silt; f—fine; m—medium; c—coarse; vc—very coarse; gr—gravel.

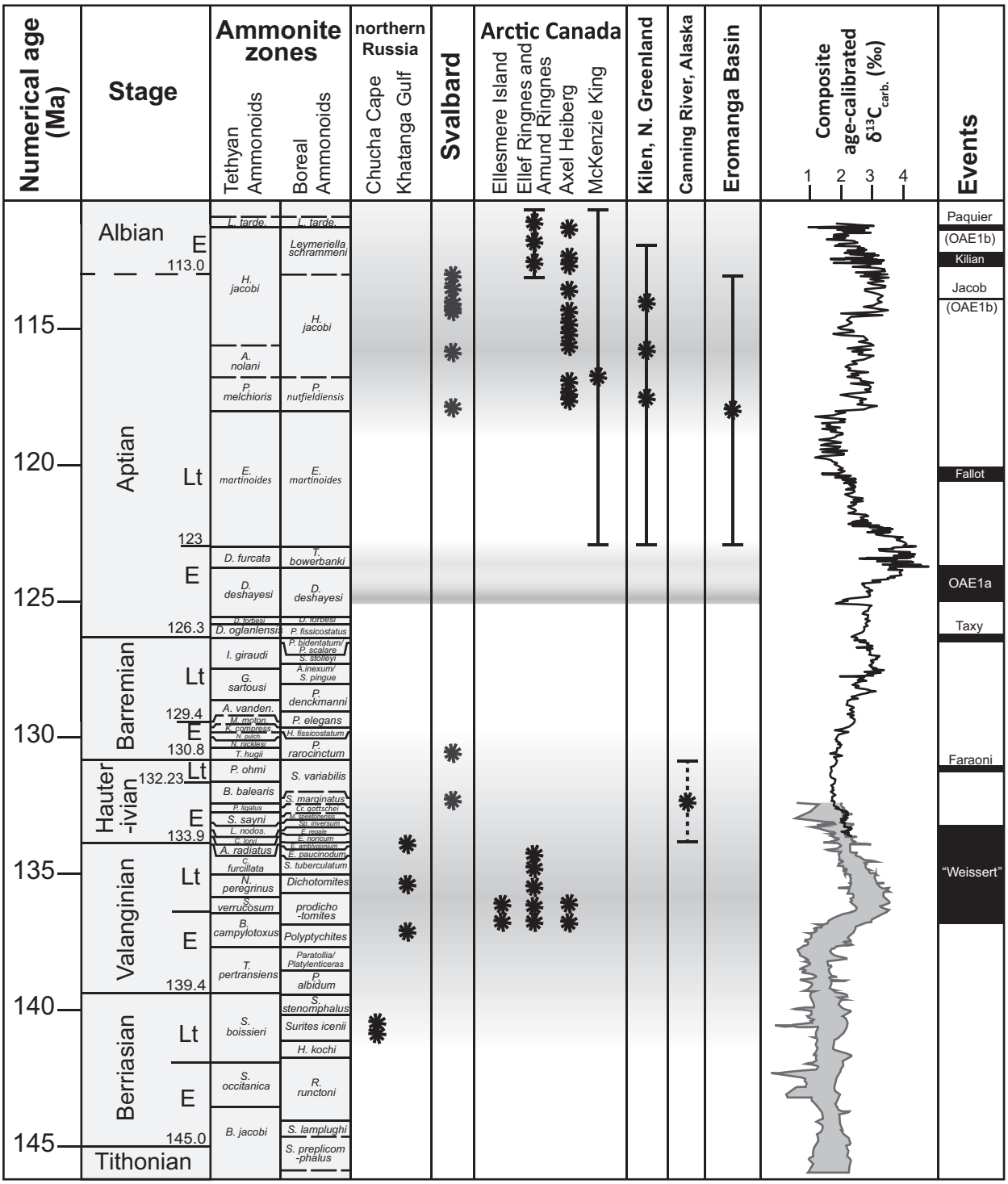

Figure 7. Correlation of glendonite occurrence in Lower Cretaceous deposits from around the globe; adapted from Rogov et al. (2017). Sources: Russia: Rogov et al. (2017); Svalbard, Norway: this study; Canadian Arctic (Queen Elizabeth Islands): Kemper and Schmitz (1975, 1981), Kemper (1987), Lippert (2004), Herrle et al. (2015), Grasby et al. (2017); Greenland: Hovikoski et al. (2018); Alaska, USA: van der Kolk et al. (2011); Eromanga Basin, Australia: Frakes et al. (1995), De Lurio and Frakes (1999). Composite $\delta^{13}C_{carbonate}$ curve constructed from Weissert and Erba (2004), Föllmi et al. (2006), Herrle et al. (2015), and Price et al. (2016); tuned to the timescale of Ogg and Hinnov (2012). Global cooling and warming episodes indicated by blue and red shaded area, respectively. Ranges indicate uncertainties in age, rather than the age range over which glendonites occur in a succession. E—early; Lt—late.

CONCLUSIONS

The glendonites from the Lower Cretaceous succession of Svalbard formed in the offshore transition zone to the shoreface of a shallow marine shelf, above SWB, suggesting water at 7 °C or lower at less than 100 m water depth, at a paleolatitude of ~60–70°N. High-resolution carbon isotope stratigraphy in conjunction with biostratigraphy enables the correlation of Early Cretaceous glendonites of Svalbard to other Early Cretaceous glendonite-bearing sites in both northern and southern high latitudes. A distinct interval of glendonites spans the late Berriasian to earliest Barremian—a duration of at least 8.6 m.y.—which pre- and post-dates the Valanginian "Weissert Event" CIE, suggesting that cooling and isotopic excursion were not mechanistically linked. The stratigraphic extent of glendonite-bearing horizons from Svalbard into the lower Barremian suggests that mid-Early Cretaceous cooling may have been significantly more prolonged (up to 8.6 m.y. duration) than has been previously suggested. Glendonites are absent from the late Barremian to early Aptian in Northern and Southern Hemisphere locations, supporting long-term warmth during this time (although regional uplift during this interval meant that it was less likely that glendonites were preserved). Glendonites reappear in the late Aptian and extend into the early Albian, corroborating other proxy evidence for late Aptian cooling. Overall, glendonites from Svalbard suggest that Cretaceous cold episodes were characterized with high latitude (>60°N) shallow water temperatures, and, if upwelling was not bringing cool waters from the North Pole these low temperatures support the existence of a northern polar ice-cap during the formation of the original ikaite.

ACKNOWLEDGMENTS

Funding for this study was provided by a Ph.D. scholarship from the University of Plymouth, UK, with additional funding to MV from the Geological Society, London, UK; The British Sedimentological Research Group Gill Harwood Memorial Fund, and an American Association of Petroleum Geologists grant-in-aid (William E. Gipson Named Grant) also to MV. We thank Dr. Marc Davis for his technical help, and Dr. Michael Bedington for his input interpreting the data. We would like to thank our editors, Ganqing Jiang and Rob Strachan, and reviewers, Dr. Mikhail Rogov and two anonymous, for their constructive criticism and advice.

REFERENCES CITED

Allen, J.R.L., 1963, The classification of cross-stratified units. With notes on their origin: Sedimentology, v. 2, p. 93–114, https://doi.org/10.1111/j.1365-3091.1963.tb01204.x.

Ando, A., Kakegawa, T., Takashima, R., and Saito, T., 2002, New perspective on Aptian carbon isotope stratigraphy: Data from $\delta^{13}C$ records of terrestrial organic matter: Geology, v. 30, p. 227–230, https://doi.org/10.1130/0091-7613(2002)030<0227:NPOACI>2.0.CO;2.

Århus, N., 1992, Some dinoflagellate cysts from the Lower Cretaceous of Spitsbergen: Grana, v. 31, p. 305–314, https://doi.org/10.1080/00173139209429453.

Bhattacharya, J.P., 2006, Deltas, *in* Posamentier, H.W., and Walker, R.G., eds., Facies Models Revisited: (SEPM) Society for Sedimentary Geology Special Publication, CD e-book no. 84, p. 237–292.

Bhattacharya, J.P., 2010, Deltas, *in* Dalrymple, R.W., and James, N.P., eds., Facies Models 4: Newfoundland, Canada, Geological Association of Canada, Geotext, v. 6, p. 233–264.

Bice, K.L., and Norris, R.D., 2002, Possible atmospheric CO_2 extremes of the Middle Cretaceous (late Albian–Turonian): Paleoceanography and Paleoclimatology, v. 17, p. 22-1–22-17.

Bice, K.L., Huber, B.T., and Norris, R.D., 2003, Extreme polar warmth during the Cretaceous greenhouse? Paradox of the late Turonian $\delta^{18}O$ record at Deep Sea Drilling Project Site 511: Paleoceanography and Paleoclimatology, v. 18, no. 2, https://doi.org/10.1029/2002PA000848.

Bischoff, J.L., Fitzpatrick, J.A., and Rosenbauer, R.J., 1993, The solubility and stabilization of ikaite ($CaCO_3{\cdot}6H_2O$) from 0° to 25° C: Environmental and paleoclimatic implications for Thinolite Tufa: The Journal of Geology, v. 101, p. 21–33, https://doi.org/10.1086/648194.

Bodin, S., Meissner, P., Janssen, N.M., Steuber, T., and Mutterlose, J., 2015, Large igneous provinces and organic carbon burial: Controls on global temperature and continental weathering during the Early Cretaceous: Global and Planetary Change, v. 133, p. 238–253, https://doi.org/10.1016/j.gloplacha.2015.09.001.

Boucot, A.J., Xu, C., and Scotese, R., 2013, Phanerozoic Paleoclimate: An Atlas of Lithologic Indicators of Climates: SEPM (Society for Sedimentary Geology), Concepts in Sedimentology and Paleontology, no. 11, Map Folio, 487 p.

Boyer, T.P., Antonov, J.I., Baranova, O.K., Coleman, C., Garcia, H.E., Grodsky, A., Johnson, D.R., Locarnini, R.A., Mishonov, A.V., O'Brien, T.D., Paver, C.R., Reagan, J.R., Seidov, D., Smolyar, I.V., and Zweng, M.M., 2013, World Ocean Database 2013, NOAA Atlas NESDIS 72: Silver Spring, Maryland, USA, U.S. Department of Commerce, National Oceanic and Atmospheric Administration, 209 p.

Brady, E.C., DeConto, R.M., and Thompson, S.L., 1998, Deep water formation and poleward ocean heat transport in the warm climate extreme of the Cretaceous (80 Ma): Geophysical Research Letters, v. 25, p. 4205–4208, https://doi.org/10.1029/1998GL900072.

Brassell, S.C., 2009, Steryl ethers in a Valanginian claystone: Molecular evidence for cooler waters in the central Pacific during the Early Cretaceous?: Palaeogeography, Palaeoclimatology, Palaeoecology, v. 282, p. 45–57, https://doi.org/10.1016/j.palaeo.2009.08.009.

Bridge, J.S., and Diemer, J.A., 1983, Quantitative interpretation of an evolving ancient river system: Sedimentology, v. 30, p. 599–623, https://doi.org/10.1111/j.1365-3091.1983.tb00698.x.

Brooks, R., Clark, L., and Thurston, E., 1950, Calcium carbonate and its hydrates: Philosophical Transactions of the Royal Society A: Mathematical, Physical and Engineering Sciences, v. 243, p. 145–167, https://doi.org/10.1098/rsta.1950.0016.

Buchardt, B., Israelson, C., Seaman, P., and Stockmann, G., 2001, Ikaite tufa towers in Ikka Fjord, southwest Greenland: Their formation by mixing of seawater and alkaline spring water: Journal of Sedimentary Research, v. 71, p. 176–189, https://doi.org/10.1306/042800710176.

Dalland, A., 1977, Erratic clasts in the Lower Tertiary deposits of Svalbard: Evidence of transport by winter ice: Arbok Norsk Polarinstitutt, v. 1976, p. 151–166.

Dalrymple, R.W., 2010, Tidal Depositional Systems, *in* Dalrymple, R.W., and James, N.P., eds., Facies Models 4: Newfoundland, Canada, Geological Association of Canada, Memorial University of Newfoundland.

De Lurio, J.L., and Frakes, L.A., 1999, Glendonites as a paleoenvironmental tool: Implications for early Cretaceous high latitude climates in Australia: Geochimica et Cosmochimica Acta, v. 63, p. 1039–1048, https://doi.org/10.1016/S0016-7037(99)00019-8.

Dieckmann, G.S., Nehrke, G., Papadimitriou, S., Göttlicher, J., Steininger, R., Kennedy, H., Wolf-Gladrow, D., Thomas, D.N., 2008, Calcium carbonate as ikaite crystals in Antarctic sea ice: Geophysical Research Letters, v. 35, no. 8, p. 1–3, https://doi.org/10.1029/2008GL033540.

Dypvik, H., Håkansson, E., and Heinberg, C., 2002, Jurassic and Cretaceous palaeogeography and stratigraphic comparisons in the North Greenland-Svalbard region: Polar Research, v. 21, p. 91–108, https://doi.org/10.1111/j.1751-8369.2002.tb00069.x.

Elliott, T., 1986, Deltas, *in* Reading, H.G., ed., Sedimentary Environments and Facies: Oxford, UK, Blackwell Scientific Publications, p. 113–154.

Erba, E., and Tremolada, F., 2004, Nannofossil carbonate fluxes during the Early Cretaceous: Phytoplankton response to nutrification episodes, atmospheric CO_2, and anoxia: Paleoceanography and Paleoclimatology, v. 19, https://doi.org/10.1029/2003PA000884.

Erba, E., Bartolini, A., and Larson, R.L., 2004, Valanginian Weissert oceanic anoxic event: Geology, v. 32, p. 149–152, https://doi.org/10.1130/G20008.1.

Ershova, E.S., 1983. Explanatory notes for the biostratigraphical scheme of the Jurassic and Lower Cretaceous deposits of Spitzbergen archipelago: Sevmorgeologia, Leningrad, v. 88 (in Russian).

Field, L., Milodowski, A.E., Shaw, R.P., Stevens, L.A., Hall, M.R., Kilpatrick, A., Gunn, J., Kemp, S.J., and Ellis, M.A., 2017, Unusual morphologies and the occurrence of pseudomorphs after ikaite ($CaCO_3{\cdot}6H_2O$) in fast growing, hyperalkaline speleothems: Mineralogical Magazine, v. 81, p. 565–590, https://doi.org/10.1180/minmag.2016.080.111.

Fluteau, F., Ramstein, G., Besse, J., Guiraud, R., and Masse, J., 2007, Impacts of palaeogeography and sea level changes on Mid-Cretaceous climate: Palaeogeography, Palaeoclimatology, Palaeoecology, v. 247, p. 357–381, https://doi.org/10.1016/j.palaeo.2006.11.016.

Föllmi, K.B., Godet, A., Bodin, S., and Linder, P., 2006, Interactions between environmental change and shallow water carbonate buildup along the northern Tethyan margin and their impact on the Early Cretaceous carbon isotope record: Paleoceanography and Paleoclimatology, v. 21, https://doi.org/10.1029/2006PA001313.

Frakes, L.A., Alley, N.F., and Deynoux, M., 1995, Early Cretaceous ice rafting and climate zonation in Australia: International Geology Review, v. 37, p. 567–583, https://doi.org/10.1080/00206819509465419.

Francis, J.E., and Poole, I., 2002, Cretaceous and early Tertiary climates of Antarctica: Evidence from fossil wood: Palaeogeography, Palaeoclimatology, Palaeoecology, v. 182, p. 47–64, https://doi.org/10.1016/S0031-0182(01)00452-7.

Frebold, H., 1928, Das Festnungsprofil auf Spitsbergen. Jura und Kreide. II, Die Stratigraphie: Skrifter om Svalbard og Ishavet, v. 19, p. 1–39.

Frebold, H., and Stoll, E., 1937, Das Festungsprofil auf Spitzbergen. III, Stratigraphie und Fauna des Jura und der Unterkreide: Skrifter om Svalbard og Ishavet, v. 68, p. 1–85.

Galloway, J.M., Sweet, A.R., Swindles, G.T., Dewing, K., Hadlari, T, Embry, A.F., and Sanei, H., 2013, Middle Jurassic to Lower Cretaceous paleoclimate of Sverdrup Basin, Canadian Arctic Archipelago inferred from the palynostratigraphy: Marine and Petroleum Geology, v. 44, p. 240–255, https://doi.org/10.1016/j.marpetgeo.2013.01.001.

Gjelberg, J., and Steel, R.J., 1995, Helvetiafjellet Formation (Barremian-Aptian), Spitsbergen: Characteristics of a transgressive succession, *in* Steel, R.J., Felt, V.L., Johannessen, E.P., and Mathieu, C., eds., Sequence Stratigraphy of the Northwest European Margin: Norwegian Petroleum Society Special Publications, v. 5, p. 571–593, https://doi.org/10.1016/S0928-8937(06)80087-1.

Grasby, S.E., McCune, G.E., Beauchamp, B., and Galloway, J.M., 2017, Lower Cretaceous cold snaps led to widespread glendonite occurrences in the Sverdrup Basin, Canadian High Arctic: Geological Society of America Bulletin, v. 129, p. 771–787, https://doi.org/10.1130/B31600.1.

Greinert, J., and Derkachev, A., 2004, Glendonites and methane-derived Mg-calcites in the Sea of Okhotsk, Eastern

Siberia: Implications of a venting-related ikaite/glendonite formation: Marine Geology, v. 204, p. 129–144, https://doi.org/10.1016/S0025-3227(03)00354-2.

Gröcke, D.R., Hesselbo, S.P., and Jenkyns, H.C., 1999, Carbon-isotope composition of Lower Cretaceous fossil wood: Ocean-atmosphere chemistry and relation to sea-level change: Geology, v. 27, p. 155–158, https://doi.org/10.1130/0091-7613(1999)027<0155:CICOLC>2.3.CO;2.

Grøsfjeld, K., 1992, Palynological age constraints on the base of the Helvetiafjellet Formation (Barremian) on Spitsbergen: Polar Research, v. 11, p. 11–19, https://doi.org/10.1111/j.1751-8369.1992.tb00408.x.

Grundvåg, S.-A., Marin, D., Kairanov, B., Śliwińska, K.K., Nøh-Hansen, H., Jelby, M.E., Escalona, A., and Olaussen, S., 2017, The Lower Cretaceous succession of the northwestern Barents Shelf: Onshore and offshore correlations: Marine and Petroleum Geology, v. 86, p. 834–857, https://doi.org/10.1016/j.marpetgeo.2017.06.036.

Harland, M., Francis, J., Brentnall, S., and Beerling, D., 2007, Cretaceous (Albian–Aptian) conifer wood from Northern Hemisphere high latitudes: Forest composition and palaeoclimate: Review of Palaeobotany and Palynology, v. 143, p. 167–196, https://doi.org/10.1016/j.revpalbo.2006.07.005.

Harland, W.B., and Kelly, S.R.A., 1997, Jurassic–Cretaceous History, *in* Harland, W.B., ed., The Geology of Svalbard: Geological Society, London, Memoir 17, p. 363–387.

Harland, W.B., Gaskell, B.A., Heaffard, A.P., Lind, E.K., and Perkins, P.J., 1984. Outline of Arctic post-Silurian continental displacements, *in* Spencer, A.M., ed., Petroleum geology of the North European Margin: London, UK, Graham and Trotman, p. 137–148, https://doi.org/10.1007/978-94-009-5626-1_10.

Haupt, B.J., and Seidov, D., 2001, Warm deep-water ocean conveyor during Cretaceous time: Geology, v. 29, p. 295–298, https://doi.org/10.1130/0091-7613(2001)029<0295:WDWOCD>2.0.CO;2.

Heimhofer, U., Hochuli, P.A., Burla, S., Andersen, N., and Weissert, H., 2003, Terrestrial carbon-isotope records from coastal deposits (Algarve, Portugal): A tool for chemostratigraphic correlation on an intrabasinal and global scale: Terra Nova, v. 15, p. 8–13, https://doi.org/10.1046/j.1365-3121.2003.00447.x.

Herrle, J.O., and Mutterlose, J., 2003, Calcareous nannofossils from the Aptian–Lower Albian of southeast France: Palaeoecological and biostratigraphic implications: Cretaceous Research, v. 24, p. 1–22, https://doi.org/10.1016/S0195-6671(03)00023-5.

Herrle, J.O., Schröder-Adams, C.J., Davis, W., Pugh, A.T., Galloway, J.M., and Fath, J., 2015, Mid-Cretaceous High Arctic stratigraphy, climate, and oceanic anoxic events: Geology, v. 43, p. 403–406, https://doi.org/10.1130/G36439.1.

Hovikoski, J., Pedersen, G.K., Alsen, P., Lauridsen, B.W., Svennevig, K., Nøhr-Hansen, H., Sheldon, E., Dybkjær, K., Bojesen-Koefoed, J., Piasecki, S., Bjerager, M., and Ineson, J., 2018, The Jurassic–Cretaceous lithostratigraphy of Kilen, Kronprins Christian Land, eastern North Greenland: Bulletin of the Geological Society of Denmark, v. 66, p. 61–112, www.2dgf.dk/publikationer/bulletin.

Hunt, J.M., 1996, Petroleum Geochemistry and Geology: New York, New York, USA, W.H. Freeman and Company, 743 p.

Hunter, S., Haywood, A., Valdes, P., Francis, J., and Pound, M., 2013, Modelling equable climates of the Late Cretaceous: Can new boundary conditions resolve data-model discrepancies?: Palaeogeography, Palaeoclimatology, Palaeoecology, v. 392, p. 41–51, https://doi.org/10.1016/j.palaeo.2013.08.009.

Hurum, J.H., Milàn, J., Hammer, O., Midtkandal, I., Amundsen, H.E.F., and Saether, B., 2006, Tracking polar dinosaurs: New finds from the Lower Cretaceous of Svalbard: Norsk Geologisk Tidsskrift, v. 86, p. 397–402.

Hurum, J.H., Druckenmiller, P.S., Hammer, Ø., Nakrem, H.A., and Olaussen, S., 2016, The theropod that wasn't: An ornithopod tracksite from the Helvetiafjellet Formation (Lower Cretaceous) of Boltodden, Svalbard, *in* Kear, B.P., Lindgren, J., Hurum, J.H., Milàn, J., and Vadja, V., eds., Mesozoic Biotas of Scandinavia and its Arctic Territories: Geological Society of London, Special Publications, v. 434, p. 189–206, https://doi.org/10.1144/SP434.10.

Ito, M., Ishigaki, A., Nishikawa, T., and Saito, T., 2001, Temporal variation in the wavelength of hummocky cross-stratification: Implications for storm intensity through Mesozoic and Cenozoic: Geology, v. 29, p. 87–89, https://doi.org/10.1130/0091-7613(2001)029<0087:TVITWO>2.0.CO;2.

Jahren, A.H., Arens, N.C., Sarmiento, G., Guerrero, J., and Amundson, R., 2001, Terrestrial record of methane hydrate dissociation in the Early Cretaceous: Geology, v. 29, p. 159–162, https://doi.org/10.1130/0091-7613(2001)029<0159:TROMHD>2.0.CO;2.

Jansen, J., Woensdregt, C., Kooistra, M., and Van Der Gaast, S., 1987, Ikaite pseudomorphs in the Zaire deep-sea fan: An intermediate between calcite and porous calcite: Geology, v. 15, p. 245–248, https://doi.org/10.1130/0091-7613(1987)15<245:IPITZD>2.0.CO;2.

Jenkyns, H.C., Forster, A., Schouten, S., and Damsté, J.S.S., 2004, High temperatures in the late Cretaceous Arctic Ocean: Nature, v. 432, p. 888–892, https://doi.org/10.1038/nature03143.

Johnsen, S.O., Mork, A., Dypvik, H., and Nagy, J., 2001, Outline of the Geology of Svalbard: Short geological review and guidebook: Syracuse, New York, USA, State University of New York, College of Environmental Science and Forestry, 7th ESF IMPACT Workshop.

Jones, T.P., and Chaloner, W.G., 1991, Fossil charcoal, its recognition and palaeoatmospheric significance: Global and Planetary Change, v. 5, p. 39–50, https://doi.org/10.1016/0921-8181(91)90125-G.

Kaljo, D., and Martma, T.O.N., 2006, Application of carbon isotope stratigraphy to dating the Baltic Silurian rocks: GFF, v. 128, p. 123–129, https://doi.org/10.1080/11035890601282123.

Kemper, E., 1987, Das Klima der Kreide-Zeit: Geologisches Jahrbuch: Reihe A, v. 96, p. 5–185.

Kemper, E., and Schmitz, H., 1975, Stellate nodules from the upper Deer Bay Formation (Valanginian) of Arctic Canada: Geological Survey of Canada, v. 75, p. 109–119, https://doi.org/10.4095/103040.

Kemper, E., and Schmitz, H.H., 1981, Glendonite: Indikatoren des polarmarinen Ablagerungsmilieus: Geologische Rundschau, v. 70, p. 759–773, https://doi.org/10.1007/BF01822149.

Koevoets, M., Abay, T., Hammer, Ø., and Olaussen, S., 2016, High-resolution organic carbon-isotope stratigraphy of the Middle Jurassic–Lower Cretaceous Agardhfjellet Formation of central Spitsbergen, Svalbard: Palaeogeography, Palaeoclimatology, Palaeoecology, v. 449, p. 266–274, https://doi.org/10.1016/j.palaeo.2016.02.029.

Lapparent, A.D., 1962, Footprints of Dinosaur in the Lower Cretaceous of Vestspitsbergen-Svalbard: Arbok Norsk Polarinstitutt, v. 1960, p. 14–21.

Lini, A., Weissert, H., and Erba, E., 1992, The Valanginian carbon isotope event: A first episode of greenhouse climate conditions during the Cretaceous: Terra Nova, v. 4, p. 374–384, https://doi.org/10.1111/j.1365-3121.1992.tb00826.x.

Lippert, P., 2004, A cold start to the Cretaceous: Defining climate history near the North Pole: Journal of Undergraduate Research, v. 2, p. 42–48.

Littler, K., Robinson, S.A., Bown, P.R., Nederbragt, A.J., and Pancost, R.D., 2011, High sea-surface temperatures during the Early Cretaceous Epoch: Nature Geoscience, v. 4, p. 169–172, https://doi.org/10.1038/ngeo1081.

Lunt, D.J., Foster, G.L., O'Brien, C.L., Pancost, R.D., and Robinson, S.A., 2016, Palaeogeographic controls on climate and proxy interpretation: Climate of the Past, v. 12, p. 1181–1198, https://doi.org/10.5194/cp-12-1181-2016.

Maher, H.D., 2001, Manifestations of the Cretaceous High Arctic Large Igneous Province in Svalbard: The Journal of Geology, v. 109, p. 91–104, https://doi.org/10.1086/317960.

Maher, H.D., Hays, T., Shuster, R., and Mutrux, J., 2004, Petrography of Lower Cretaceous sandstones on Spitsbergen: Polar Research, v. 23, p. 147–165, https://doi.org/10.1111/j.1751-8369.2004.tb00005.x.

Martinez, M., Deconinck, J.-F., Pellenard, P., Riquier, L., Company, M., Reboulet, S., and Moiroud, M., 2015, Astrochronology of the Valanginian–Hauterivian stages (Early Cretaceous): Chronological relationships between the Paraná–Etendeka large igneous province and the Weissert and the Faraoni events: Global and Planetary Change, v. 131, p. 158–173, https://doi.org/10.1016/j.gloplacha.2015.06.001.

Maurer, F., van Buchem, F.S.P., Eberli, G.P., Pierson, B.J., Raven, M.J., Larsen, P-H., Al-Husseini, M.I., and Vincent, B., 2013, Late Aptian long-lived glacio-eustatic lowstand recorded on the Arabian Plate: Terra Nova, v. 25, p. 87–94, https://doi.org/10.1111/ter.12009.

McAnena, A., Hofmann, S.F.P., Herrie, J.O., Griesand, A., Pross, J., Talbot, H.M., Rethemeyer, J., Wallmann, K., and Wagner, T., 2013, Atlantic cooling associated with a marine biotic crisis during the mid-Cretaceous period: Nature Geoscience, v. 6, p. 558–561, https://doi.org/10.1038/ngeo1850.

McArthur, J., Janssen, N.M.M., Reboulet, S., Leng, M.J., Thirlwall, M.F., and van de Schootbrugge, B., 2007, Palaeotemperatures, polar ice-volume, and isotope stratigraphy (Mg/Ca, $\delta^{18}O$, $\delta^{13}C$, $^{87}Sr/^{86}Sr$): The Early Cretaceous (Berriasian, Valanginian, Hauterivian): Palaeogeography, Palaeoclimatology, Palaeoecology, v. 248, p. 391–430, https://doi.org/10.1016/j.palaeo.2006.12.015.

Meissner, P., Mutterlose, J., and Bodin, S., 2015, Latitudinal temperature trends in the northern hemisphere during the Early Cretaceous (Valanginian–Hauterivian): Palaeogeography, Palaeoclimatology, Palaeoecology, v. 424, p. 17–39, https://doi.org/10.1016/j.palaeo.2015.02.003.

Menegatti, A.P., Weissert, H., Brown, R.S., Tyson, R.V., Farrimond, P., Strasser, A., and Caron, M., 1998, High-resolution $\delta^{13}C$ stratigraphy through the Early Aptian "Livello selli" of the Alpine tethys: Paleoceanography and Paleoclimatology, v. 13, p. 530–545, https://doi.org/10.1029/98PA01793.

Miall, A.D., 1985, Architectural-element analysis: A new method of facies analysis applied to fluvial deposits: Earth-Science Reviews, v. 22, p. 261–308, https://doi.org/10.1016/0012-8252(85)90001-7.

Midtkandal, I., and Nystuen, J., 2009, Depositional architecture of a low-gradient ramp shelf in an epicontinental sea: The lower Cretaceous of Svalbard: Basin Research, v. 21, p. 655–675, https://doi.org/10.1111/j.1365-2117.2009.00399.x.

Midtkandal, I., Nystuen, J.P., Nagy, J., and Mørk, A., 2008, Lower Cretaceous lithostratigraphy across a regional subaerial unconformity in Spitsbergen: The Rurikfjellet and Helvetiafjellet formations: Norsk Geologisk Tidsskrift, v. 88, p. 287–304.

Midtkandal, I., Svensen, H., Planke, S., Corfu, F., Polteau, S., Torsvik, T., Faleide, J.I., Grundvåg, S.-A., Selnes, H., and Olaussen, S., 2016, The Aptian oceanic anoxic event (OAE1a) in Svalbard and the age of the Barremian-Aptian boundary: European Geosciences Union General Assembly 2016, Vienna, Austria, April 17–22, Geophysical Research Abstracts, v. 18, no. EGU2016-14744.

Millán, M., Weissert, H., and López-Horgue, M., 2014, Expression of the late Aptian cold snaps and the OAE1b in a highly subsiding carbonate platform (Aralar, northern Spain): Palaeogeography, Palaeoclimatology, Palaeoecology, v. 411, p. 167–179, https://doi.org/10.1016/j.palaeo.2014.06.024.

Morales, C., Rogov, M., Wierzbowski, H., Ershova, V., Suan, G., Adatte, T., Föllmi, K.B., Tegelaar, E., Reichart, G.-J., de Lange, G.J., Middelburg, J.J., and van de Schootbrugge, B., 2017, Glendonites track methane seepage in Mesozoic polar seas: Geology, v. 45, p. 503–506, https://doi.org/10.1130/G38967.1.

Mørk, A., and Worsley, D., 2006, The Festningen section: Norsk Geologisk Forening (NGF) abstracts and proceedings, v. 3, p. 31–35.

Mørk, A., Dallmann, W.K., and Dypvik, H., 1999. Mesozoic lithostratigraphy, *in* Dallmann W.K., ed., Lithostratigraphic Lexicon of Svalbard, Review and Recommendations for Nomenclature Use: Upper Paleozoic to Quaternary Bedrock: Tromsø, Norway, Norwegian Polar Institute, p. 127–214.

Mutterlose, J., and Kessels, K., 2000, Early Cretaceous calcareous nannofossils from high latitudes: Implications for palaeobiogeography and palaeoclimate: Palaeogeography, Palaeoclimatology, Palaeoecology, v. 160, p. 347–372, https://doi.org/10.1016/S0031-0182(00)00082-1.

Mutterlose, J., Bornemann, A., and Herrle, J., 2009, The Aptian–Albian cold snap: Evidence for "mid" Cretaceous icehouse interludes: Neues Jahrbuch für Geologie und Palaontologie. Abhandlungen, v. 252, p. 217–225, https://doi.org/10.1127/0077-7749/2009/0252-0217.

Mutterlose, J., Malkoc, M., Schouten, S., Sinninghe Damsté, J.S., and Forster, A., 2010, TEX86 and stable $\delta^{18}O$ paleothermometry of early Cretaceous sediments: Implications for belemnite ecology and paleotemperature proxy application: Earth and Planetary Science Letters, v. 298, p. 286–298, https://doi.org/10.1016/j.epsl.2010.07.043.

Nagy, J., 1970, Ammonite faunas and stratigraphy of Lower Cretaceous (Albian) rocks in southern Spitsbergen: Norsk Polarinstitutt Skrifter 152, 58 p.

Nejbert, K., Krajewski, K.P., Dubińska, E., and Pécskay, Z., 2011, Dolerites of Svalbard, north-west Barents Sea Shelf: Age, tectonic setting and significance for geotectonic interpretation of the High-Arctic Large Igneous Province: Polar Research, v. 30, no. 7306, https://doi.org/10.3402/polar.v30i0.7306.

Ogg, J.G., and Hinnov, L.A., 2012, Cretaceous, *in* Gradstein, F.M., Ogg, G., and Schmitz, M., eds., The Geological Timescale: Boston, Massachusetts, USA, Elsevier, p. 793–853, https://doi.org/10.1016/B978-0-444-59425-9.00027-5.

Parker, J.R., 1967, The Jurassic and Cretaceous sequence in Spitsbergen: Geological Magazine, v. 104, p. 487–505, https://doi.org/10.1017/S0016756800049220.

Patruno, S., Hampson, G.J., and Jackson, C.A., 2015, Quantitative characterisation of deltaic and subaqueous clinoforms: Earth-Science Reviews, v. 142, p. 79–119, https://doi.org/10.1016/j.earscirev.2015.01.004.

Peters, K.E., Walters, C.C., and Moldowan, J.M., 2005, The Biomarker Guide, part 2, Biomarkers in Petroleum Exploration and Earth History: Cambridge, UK, Cambridge University Press, v. 2, p. 475–983.

Peters, S.E., and Loss, D.P., 2012, Storm and fair-weather wave base: A relevant distinction?: Geology, v. 40, p. 511–514, https://doi.org/10.1130/G32791.1.

Plint, A.G., 2010, Wave- and storm-dominated shoreline and shallow-marine systems, *in* James, N.P., and Dalrymple, R.W., eds., Facies Models 4: Newfoundland, Canada, Geological Association of Canada, Memorial University of Newfoundland.

Polteau, S., Hendriks, B.W.H., Planke, S., Ganerød, M., Corfuc, F., Faleide, J.I., Midtkandal, I., Svensen, H.S., and Myklebust, R.,, 2016, The Early Cretaceous Barents Sea Sill Complex: Distribution, $^{40}Ar/^{39}Ar$ geochronology, and implications for carbon gas formation: Palaeogeography, Palaeoclimatology, Palaeoecology, v. 441, p. 83–95, https://doi.org/10.1016/j.palaeo.2015.07.007.

Price, G., and Mutterlose, J., 2004, Isotopic signals from late Jurassic–early Cretaceous (Volgian–Valanginian) sub-Arctic belemnites, Yatria River, Western Siberia: Journal of the Geological Society, v. 161, p. 959–968, https://doi.org/10.1144/0016-764903-169.

Price, G.D., and Nunn, E.V., 2010, Valanginian isotope variation in glendonites and belemnites from Arctic Svalbard: Transient glacial temperatures during the Cretaceous greenhouse: Geology, v. 38, p. 251–254, https://doi.org/10.1130/G30593.1.

Price, G.D., and Passey, B.H., 2013, Dynamic polar climates in a greenhouse world: Evidence from clumped isotope thermometry of Early Cretaceous belemnites: Geology, v. 41, p. 923–926, https://doi.org/10.1130/G34484.1.

Price, G.D., Sellwood, B., and Valdes, P., 1995, Sedimentological evaluation of general circulation model simulations for the "greenhouse" Earth: Cretaceous and Jurassic case studies: Sedimentary Geology, v. 100, p. 159–180, https://doi.org/10.1016/0037-0738(95)00106-9.

Price, G.D., Fozy, I., and Pálfy, J., 2016, Carbon cycle history through the Jurassic–Cretaceous boundary: A new global $\delta^{13}C$ stack: Palaeogeography, Palaeoclimatology, Palaeoecology, v. 451, p. 46–61, https://doi.org/10.1016/j.palaeo.2016.03.016.

Pucéat, E., Lécuyer, C., Sheppard, S.M.F., Dromart, G., Reboulet, S., and Grandjean, P., 2003, Thermal evolution of Cretaceous Tethyan marine waters inferred from oxygen isotope composition of fish tooth enamels: Paleoceanography and Paleoclimatology, v. 18, no. 2, https://doi.org/10.1029/2002PA000823.

Purgstaller, B., Dietzel, M., Baldermann, A., and Mavromatis, V., 2017, Control of temperature and aqueous Mg^{2+}/Ca^{2+} ratio on the (trans-) formation of ikaite: Geochimica et Cosmochimica Acta, v. 217, p. 128–143, https://doi.org/10.1016/j.gca.2017.08.016.

Radke, M., and Welte, D.H., 1983, The Methylphenanthrene Index (MPI): A maturity parameter based on aromatic hydrocarbons, *in* Bjorøy, M., Albrecht, C., Cornford, C., et al., eds., Advances in Organic Geochemistry 1981: New York, USA, John Wiley & Sons, p. 504–512.

Reading, H.G., 1996, Sedimentary Environments: Processes, Facies and Stratigraphy: Oxford, UK, Blackwell Science Ltd.

Rodríguez-López, J.P., Liesa, C.L., Pardo, G., Meléndez, N., Soria, A.R., and Skilling, I., 2016, Glacial dropstones in the western Tethys during the late Aptian–early Albian cold snap: Palaeoclimate and palaeogeographic implications for the mid-Cretaceous: Palaeogeography, Palaeoclimatology, Palaeoecology, v. 452, p. 11–27, https://doi.org/10.1016/j.palaeo.2016.04.004.

Rogov, M.A., Ershova, V.B., Shchepetova, E.V., Zakharov, V.A., Pokrovsky, B.G., and Khudoley, A.K., 2017, Earliest Cretaceous (late Berriasian) glendonites from Northeast Siberia revise the timing of initiation of transient Early Cretaceous cooling in the high latitudes: Cretaceous Research, v. 71, p. 102–112, https://doi.org/10.1016/j.cretres.2016.11.011.

Schubert, C., Nürnberg, D., Scheele, N., Pauer, F., and Kriews, M., 1997, 13C isotope depletion in ikaite crystals: Evidence for methane release from the Siberian shelves?: Geo-Marine Letters, v. 17, p. 169–174, https://doi.org/10.1007/s003670050023.

Selleck, B.W., Carr, P.F., and Jones, B.G., 2007, A review and synthesis of glendonites (pseudomorphs after ikaite) with new data: Assessing applicability as recorders of ancient coldwater conditions: Journal of Sedimentary Research, v. 77, p. 980–991, https://doi.org/10.2110/jsr.2007.087.

Senger, K., Tveranger, J., Ogata, K., Braathen, A., and Planke, S., 2014, Late Mesozoic magmatism in Svalbard: A review: Earth-Science Reviews, v. 139, p. 123–144, https://doi.org/10.1016/j.earscirev.2014.09.002.

Simpson, J.H., and Sharples, J., 2012, Introduction to the Physical and Biological Oceanography of Shelf Seas: Cambridge, UK, Cambridge University Press, https://doi.org/10.1017/CBO9781139034098.

Sokolov, D., and Bodylevsky, W., 1931, Juraund Kreideformationen von Spitzbergen: Skrifter om Svalbard og Ishavet, v. 35, p. 1–151.

Spielhagen, R.F., and Tripati, A., 2009, Evidence from Svalbard for near-freezing temperatures and climate oscillations in the Arctic during the Paleocene and Eocene: Palaeogeography, Palaeoclimatology, Palaeoecology, v. 278, p. 48–56, https://doi.org/10.1016/j.palaeo.2009.04.012.

Steel, R., Gjelberg, J., and Haarr, G., 1978, Helvetiafjellet Formation (Barremian) at Festningen, Spitsbergen; a field guide: Norsk Polarinstitutt Årbok, v. 1977, p. 111–128.

Stewart, R.H., 2008, Introduction to Physical Oceanography: Department of Oceanography, College Station, Texas, USA, Texas A&M University, http://hdl.handle.net/1969.1/160216.

Stockmann, G., Tollefsen, E., Skelton, A., Brüchert, V., Balic-Zunic, T., Langhof, J., Skogby, H., and Karlsson, A., 2018, Control of a calcite inhibitor (phosphate) and temperature on ikaite precipitation in Ikka Fjord, southwest Greenland: Applied Geochemistry, v. 89, p. 11–22, https://doi.org/10.1016/j.apgeochem.2017.11.005.

Suan, G., Van De Schootbrugge, B., Adatte, T., Fiebig, J., and Oschmann, W., 2015, Calibrating the magnitude of the Toarcian carbon cycle perturbation: Paleoceanography and Paleoclimatology, v. 30, p. 495–509, https://doi.org/10.1002/2014PA002758.

Suess, E., Balzer, W., Hesse, K.-F., Müller, P.J., Ungerer, C.A., and Wefer, G., 1982, Calcium carbonate hexahydrate from organic-rich sediments of the Antarctic shelf: Precursors of glendonites: Science, v. 216, p. 1128–1131, https://doi.org/10.1126/science.216.4550.1128.

Swainson, I.P., and Hammond, R.P., 2001, Ikaite, CaCO3·6H2O: Cold comfort for glendonites as paleothermometers: American Mineralogist, v. 86, p. 1530–1533, https://doi.org/10.2138/am-2001-11-1223.

Teichert, B., and Luppold, F., 2013, Glendonites from an Early Jurassic methane seep: Climate or methane indicators?: Palaeogeography, Palaeoclimatology, Palaeoecology, v. 390, p. 81–93, https://doi.org/10.1016/j.palaeo.2013.03.001.

Thomas, R.G., Smith, D.G., Wood, J.M., Visser, J., Calverley-Range, E.A., and Koster, E.H., 1987, Inclined heterolithic stratification: Terminology, description, interpretation and significance: Sedimentary Geology, v. 53, p. 123–179, https://doi.org/10.1016/S0037-0738(87)80006-4.

Thusu, B., 1978, Aptian to Toarcian dinoflagellate cysts from Arctic Norway: Continental shelf Institute Publications, v. 100, p. 61–95.

Tissot, B.P., and Welte, D.H., 1984, Petroleum Formation and Occurrence: Berlin, Germany, Springer-Verlag, 699 p., https://doi.org/10.1007/978-3-642-87813-8.

Turney, C., Wheeler, D., and Chivas, A.R., 2006, Carbon isotope fractionation in wood during carbonization: Geochimica et Cosmochimica Acta, v. 70, p. 960–964, https://doi.org/10.1016/j.gca.2005.10.031.

Tyson, R.V., 1995, Sedimentary Organic Matter: London, UK, Chapman and Hall, https://doi.org/10.1007/978-94-011-0739-6.

van der Kolk, D.A., Whalen, M.T., Wartes, M.A., Newberry, R.J., and McCarthy, P., 2011, Geology and Source Rock Potential of the Lower Cretaceous Pebble Shale Unit, Northeastern Alaska: American Association of Petroleum Geologists Pacific Section Meeting, May 8–11, Anchorage, Alaska, USA, Search and Discovery Article 90125.

Vickers, M.L., Price, G.D., Jerrett, R.M., and Watkinson, M., 2016, Stratigraphic and geochemical expression of Barremian–Aptian global climate change in Arctic Svalbard: Geosphere, v. 12, p. 1594–1605, https://doi.org/10.1130/GES01344.1.

Vickers, M., Watkinson, M., Price, G.D., and Jerrett, R., 2018, An improved model for the ikaite-glendonite transformation: Evidence from the Lower Cretaceous of Spitsbergen, Svalbard: Norsk Geologisk Tidsskrift, v. 98, p. 1–15, https://doi.org/10.17850/njg98-1-01.

Wang, Y., Huang, C., Sun, B., Quan, C., Wu, J., and Lin, Z., 2014, Paleo-CO2 variation trends and the Cretaceous greenhouse climate: Earth-Science Reviews, v. 129, p. 136–147, https://doi.org/10.1016/j.earscirev.2013.11.001.

Webb, B., Clack, P., and Walling, D., 2003, Water-air temperature relationships in a Devon river system and the role of flow: Hydrological Processes, v. 17, p. 3069–3084, https://doi.org/10.1002/hyp.1280.

Weissert, H., and Erba, E., 2004, Volcanism, CO2 and palaeoclimate: A Late Jurassic–Early Cretaceous carbon and oxygen isotope record: Journal of the Geological Society, v. 161, p. 695–702, https://doi.org/10.1144/0016-764903-087.

Wood, G., Gabriel, A. and Lawson, J., 1996, Palynological techniques: Processing and microscopy: Palynology: Principles and Applications, v. 1, p. 29–50.

Worsley, D., 2008, The post-Caledonian development of Svalbard and the western Barents Sea: Polar Research, v. 27, p. 298–317, https://doi.org/10.1111/j.1751-8369.2008.00085.x.

Yang, D., and Peterson, A., 2017, River water temperature in relation to local air temperature in the Mackenzie and Yukon Basins: Arctic, v. 70, p. 47–58, https://doi.org/10.14430/arctic4627.

Zabel, M., and Schulz, H.D., 2001, Importance of submarine landslides for non-steady state conditions in pore water systems: Lower Zaire (Congo) deep-sea fan: Marine Geology, v. 176, p. 87–99, https://doi.org/10.1016/S0025-3227(01)00164-5.

Zhou, X., Lu, Z., Rickaby, R.E.M., Domack, E.W., Wellner, J.S., and Kennedy, H.A., 2015, Ikaite abundance controlled by porewater phosphorus level: Potential links to dust and productivity: The Journal of Geology, v. 123, p. 269–281, https://doi.org/10.1086/681918.

Science Editor: Rob Strachan
Associate Editor: Ganqing Jiang

Manuscript Received 3 July 2018
Revised Manuscript Received 16 January 2019
Manuscript Accepted 27 February 2019

Printed in the USA